A computational study of robust formation of spatial protein patterns

Sokolowski, T.R.

2013

Chapter 2

1D-eGFRD

2.1 Introduction to eGFRD

Green's Function Reaction Dynamics, in short GFRD, is a next-event driven stochastic simulation algorithm for chemical reactions in time and space that retains spatial information on the particle level. The original motivation for GFRD was the limited availability of techniques that combine the efficiency of zero-dimensional next-event driven algorithms, such as the Stochastic Simulation Algorithm by Gillespie [53, 54], with the richness of detail provided by particle-based schemes like Brownian Dynamics, which however are computationally demanding. At its heart, GFRD decomposes the simulated volume into geometrically simple subvolumes ("domains") that contain at most two particles in order to sample next-events from Green's functions, i.e. exact analytical solutions of the reaction-diffusion problem. The Green's functions are used to compute next-event times and particle positions in runtime, updating the individual domains in an asynchronous fashion. Thanks to the complete knowledge of the expected spatio-temporal evolution of the probability density within each domain, large jumps in time and space can be performed and sampling of particle trajectories is unneccessary. In terms of computational effort, GFRD is orders of magnitudes more efficient than brute-force Brownian Dynamics for biologically relevant particle concentrations ($c \leq 1\ \mu M$) [42].

Originally, GFRD was developed by van Zon and ten Wolde in 2005 [39, 40, 41]. While this first version successfully implemented the basic idea of GFRD, it employed Green's functions that were calculated under the assumption that interacting particles can separate infinitely far. This required the definition of a maximum time step and distance-cutoff, in order to ensure that interactions with particles further away than the closest particle indeed can be neglected. Hence, the original scheme was event-driven, but not exact, and updates were synchronous. In 2010 Tănase-Nicola, Takahashi and ten Wolde presented an improved version of the algorithm, called eGFRD (e for enhanced) [42], inspired by earlier work [55, 56]. Here the necessity for a time cutoff was eliminated by the use of Green's functions with absorbing boundary conditions on the outer radii of the spherical domains. While this approach demands the calculation of Green's functions that are more complicated, it guarantees that

any sampled next-event occurs within the domain, and thus truly breaks down the N-particle problem into independent one- and two-particle problems. This makes eGFRD an exact, event-driven, asynchronous algorithm.

GFRD proved an extremly powerful tool to simulate diffusion and reactions of spherical particles in an unbounded three-dimensional volume [42, 41]. However, as yet it did not allow for the simulation of transport on one- and two-dimensional structures, which play a prominent role in many intracellular processes, such as DNA sliding and active transport on microtubules or actin filaments, and reactions at the cell membrane. Here we present work that extends eGFRD in a way that enables the simulation of transport and particle reactions on finite structures in 1D, 2D and 3D, and transitions between the 3D bulk and the lower-dimensional structures.

The following content is organized as follows: First we describe the working principles of eGFRD in more detail. Thereby we introduce common GFRD terminology. After that, in section 2.2 we explain how we include transport and reactions on 1D structures into eGFRD, introducing new, cylindrical domain types. These require new Green's functions, and a large part of this chapter is indeed devoted to their mathematical derivation. This will be conducted in detail for the most important case in section 2.3 and provides an exemplary reference for other cases presented in this and later chapters. Where instructive, methodic details of Green's function calculation will be mentioned. For a complete overview of the use of Green's functions in solving the diffusion/heat equation we refer to the classical book by Carslaw & Jaeger [57] and [58, 59], which are excellent sources. Section 2.4 briefly introduces additional modifications that are necessary to model linear tracks of finite length. To end with, in section 2.5 we present a Green's function used to model diffusive transport in 1D in the presence of a reactive sink.

The implementation of 2D transport into eGFRD is discussed separately in Chapter 2 and partly builds on what follows in this chapter.

2.1.1 Working principle of eGFRD

Imagine a random constellation of N particles of different chemical species that diffuse and react in a 3D volume. Let us assume that the particles are well-represented by solid spherical spheres and completely characterized by their radius, diffusion constant, rates of interaction with each other and their decay rate. Even with these simplifications, in general it is hard–if not impossible–to find an analytical prediction for future particle species and positions given that the system started from a certain initial condition. Nonetheless, as often in physics, exact analytical solutions can be obtained for the case $N \leq 2$. eGFRD capitalizes on this fact by dividing the 3D volume into subvolumes, called protective domains, that contain at most two particles, in order to isolate the content of each domain from the influence of surrounding particles up to a certain (domain-specific) time $\tau_{\mathcal{D}}$. This way the N-particle problem is reduced to $M < N$ independent one- or two-particle problems. $\tau_{\mathcal{D}}$ is the time at which a reconstruction of the domain becomes necessary, e.g. when one of the particles hits a domain boundary or experiences a reaction that changes its properties. Figure 2.1 illustrates this principle.

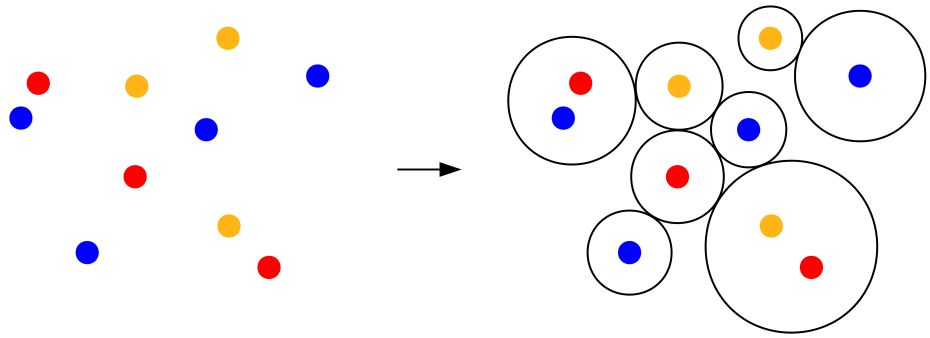

Figure 2.1: Protective domains separate the N-particle problem into one- and two-particle problems. The drawing illustrates how eGFRD constructs protective domains that contain at most two particles in order to isolate these from the influence of other particles, starting from a random particle constellation. Subsequently, analytical solutions are calculated for each domain individually and used to propagate the domains in an event-driven, asynchronous fashion. We show here a 2D projection for the standard scenario in which particles diffuse and react in unbounded 3D space. In this case protective domains are spherical. Different colors mark different chemical species.

For sufficiently simple domain geometries, such as spheres or cylinders, the Green's functions for the isolated reaction-diffusion problems, i.e. the density function $p(\mathbf{r}, t|\mathbf{r}_0)$ for the probability that a particle is at position $\mathbf{r}$ at time t given that it started at position $\mathbf{r}_0$, can be calculated analytically with exact results. Here the confining character of the domain is taken into account by imposing specific boundary conditions to $p(\mathbf{r}, t|\mathbf{r}_0)$. Quantities that derive from the Green's function can be used to generate tentative next-event times for each domain individually. Most importantly, since $p(\mathbf{r}, t|\mathbf{r}_0)$ completely describes the transient dynamics within the domain, it enables the sampling of new particle positions at $\tau_{\mathcal{D}}$, rendering the sampling of particle trajectories unnecessary. If collected in an global scheduler list, the sampled times can be used to update the domains sequentially, i.e. asynchronously, and to set up an event-driven scheme. While updates result in particle displacements and possibly species changes, by construction these remain confined to the respective domain and thus do not interfere with the situation in neighboring domains. After each domain update the domain is removed, the new constellation of particles is reanalysed and new domains are constructed around the displaced particles. The newly calculated next-event times are inserted into the ordered scheduler in the right place and the domain with the foremost next-event time is updated next. To enhance the formation of two-particle domains, recently updated particles can force a premature update of domains in their proximity, called "bursting". A bursted domain is propagated towards a time prior to its originally scheduled update; the new particle position at that time sampled form the associated Green's function. If bursting causes particles to move close enough, creation of a two-particle domain will be attempted. A compact overview over the basic eGFRD algorithm is given by Algorithm 1.

Algorithm 1 Basic outline of the eGFRD algorithm. Symbols $\mathcal{D}_\mathrm{x}$ denote domains, τ_x next-event times. The scheduler S is the list of all next-event times in the system, ordered by increasing time. List U collects all particles that have been updated at a given time τ_x and require construction of a new domain. t_sim is the time that passed since simulation start.

Initialize:
$t_\mathrm{sim} \leftarrow 0$, scheduler $S \leftarrow \{\}$
for all particles p_i **do**
  if not p_i already in domain **then**
    $\mathcal{D}_\mathrm{j} \leftarrow$ create domain for p_i
    $\tau_\mathrm{j} \leftarrow$ draw next-event time for $\mathcal{D}_\mathrm{j}$
    insert τ_j into S ordered by increasing time
  end if
end for

Main loop:
while $S \neq \{\}$ **and** $t_\mathrm{sim} < t_\mathrm{end}$ **do**
  $t_\mathrm{sim} \leftarrow \tau_\mathrm{n} =$ topmost element in S
  remove τ_n from S
  propagate $\mathcal{D}_\mathrm{n}$ to τ_n and remove $\mathcal{D}_\mathrm{n}$
  reset particle update list: $U \leftarrow \{\}$
  $U \leftarrow U \cup \{p_{\mathrm{n}_\mathrm{i}}\}$ **for all** particles $p_{\mathrm{n}_\mathrm{i}} \in \mathcal{D}_\mathrm{n}$
  while $U \neq \{\}$ **do**
    $p_\mathrm{u} \leftarrow$ next particle in U
    for all domains $\mathcal{D}_{\mathrm{u}_\mathrm{j}}$ close to p_u **do**
      burst: propagate $\mathcal{D}_{\mathrm{u}_\mathrm{j}}$ to τ_n and remove $\mathcal{D}_{\mathrm{u}_\mathrm{j}}$
      remove $\tau_{\mathrm{u}_\mathrm{j}}$ from S
      $U \leftarrow U \cup \{p_{\mathrm{u}_\mathrm{jk}}\}$ **for all** particles $p_{\mathrm{u}_\mathrm{jk}} \in \mathcal{D}_{\mathrm{u}_\mathrm{j}}$
    end for
  end while
  for all $p_\mathrm{u} \in U$ **do**
    if not p_u already in domain **then**
      $\mathcal{D}_\mathrm{u} \leftarrow$ create domain for p_u
      $\tau_\mathrm{u} \leftarrow$ draw next-event time for $\mathcal{D}_\mathrm{u}$
      insert τ_u into S
    end if
  end for
end while

In the following we will call domains that contain one particle *Single* domains or *Singles* and domains that contain two particles *Pair* domains or *Pairs*. We will now explain how Green's functions may be used to sample next-event times for the two domain types specifically.

2.1.2 Single domains

Two types of next-events can happen within a *Single* domain $\mathcal{D}_1$: either the particle undergoes a monomolecular reaction, which can mean decay or species change, or it hits the boundary of the domain by diffusion. In eGFRD, the former is called a *Single Reaction*, the latter a *Single Escape*.

If we assume that monomolecular reactions are a Poissonian process independent of particle diffusion, the propensity function for the next reaction is simply an exponential distribution

$$q_{\mathrm{m}}(t) = k_{\mathrm{m}} e^{-k_{\mathrm{m}} t} \tag{2.1}$$

where k_{m} is the rate of the specific monomolecular reaction. A tentative next-event time τ_{m} for a monomolecular reaction then can be sampled via the inversion method as

$$\tau_{\mathrm{m}} = -k_{\mathrm{m}} \ln(\mathcal{R}_{\mathrm{m}}) \tag{2.2}$$

where $\mathcal{R}_{\mathrm{m}} \in [0, 1]$ is a uniformely distributed random number.

Let $p(\mathbf{r}, t|\mathbf{r}_0)$ be the density function for the probability that a diffusing particle will be located at $\mathbf{r}$ at time t given that it started at $\mathbf{r}_0$ at time $t_0 = 0$. Within an unbounded volume, the evolution of $p(\mathbf{r}, t|\mathbf{r}_0)$ is well-described by the diffusion equation

$$\partial_{\mathrm{t}} p(\mathbf{r}, t|\mathbf{r}_0) = D\nabla^2 p(\mathbf{r}, t|\mathbf{r}_0) + \delta(\mathbf{r} - \mathbf{r}_0)\delta(t - t_0) \quad . \tag{2.3}$$

Note that due to the delta-peak inhomogeneity that represents the initial condition, the solution $p(\mathbf{r}, t|\mathbf{r}_0)$ technically is a Green's function.

To sample a first-passage time for the particle to reach the outer shell $\partial\mathcal{D}_1$ of a domain $\mathcal{D}_1$ constructed around $\mathbf{r}_0$, additionally an absorbing boundary condition may be imposed as follows:

$$p(\mathbf{r}, t|\mathbf{r}_0) = 0 \quad \text{for} \quad \mathbf{r} \in \partial\mathcal{D}_1 \tag{2.4}$$

In the simplest case, for a spherical domain with radius R:

$$p(|\mathbf{r} - \mathbf{r}_0| = R, t|\mathbf{r}_0) = 0 \tag{2.5}$$

For more complicated domain geometries, e.g. cylinders, the problem has to be transformed into a coordinate system that captures specific symmetries, and boundary conditions have to be imposed for each coordinate separately.

Given that the Green's function $p(\mathbf{r}, t|\mathbf{r}_0)$ for the above boundary-value problem can be found, integration of $p(\mathbf{r}, t|\mathbf{r}_0)$ over the whole domain yields its survival probability $S(t)$, i.e. the probability for the particle(s) to still remain within $\mathcal{D}_1$ at time t.

Note that $S(t_0) = 1$. The survival probability is linked to the propensity function $q(t)$, which is the probability for hitting $\partial\mathcal{D}_1$ within the time interval $[t, t+dt]$, via:

$$q(t) = -\partial_t S(t) = -\partial_t \int_{\mathcal{D}_1} p(\mathbf{r}, t|\mathbf{r}_0) d\mathbf{r} \tag{2.6}$$

In other words, $1 - S(t) = \int_{t_0}^{t} q(t')dt' = Q(t)$ is equal to the cumulative distribution function of $q(t)$ and may be used to sample a next-event time τ_e for exiting the domain via the inversion method as follows:

$$\tau_e = Q^{-1}(\mathcal{R}_e) = S^{-1}(1 - \mathcal{R}_e) \tag{2.7}$$

Here $\mathcal{R}_e \in [0, 1]$ again is a uniformely distributed random number. In general, it may be difficult to calculate S^{-1} analytically. Then τ_e can be obtained by solving the equation $S(\tau_e) - \mathcal{R}_e = 0$ with a numerical rootfinder[1].

After construction of an eGFRD *Single* domain, first both τ_e and τ_m are sampled as described. Since we presuppose that diffusion and monomolecular reactions are occuring independently, the next-event time for the domain is set as:

$$\tau_{\mathcal{D}_1} = \min(\tau_e, \tau_m) \tag{2.8}$$

This automatically determines the event type to be either a *Single Escape* or a *Single Reaction*. For reasons discussed earlier and in appendix section 2.B.2, eGFRD also allows for "bursting", i.e. update of the domain at times $\tau_b < \tau_{\mathcal{D}_1}$. Here we make use of the fact that eGFRD is capable to generate a new particle position $\mathbf{r}_\nu$ from the Green's function for an arbitrary update time $\tau_\nu \leq \tau_{\mathcal{D}_1}$. Since in these cases the PDF $p(\mathbf{r}, \tau_\nu|\mathbf{r}_0)$ is not normalized within $\mathcal{D}_1$, precisely because probability leaked out through $\partial\mathcal{D}_1$ during the time $\tau_\nu - t_0$, it is important to sample $\mathbf{r}_\nu$ from the conditional PDF $p_{S(\tau_\nu)}(\mathbf{r}, \tau_\nu|\mathbf{r}_0) \equiv \frac{1}{S(\tau_\nu)} p(\mathbf{r}, \tau_\nu|\mathbf{r}_0)$. How this is done in detail depends on the geometry of the domain. For a spherical domain with radius R the angles $\theta \in [0, \pi]$ and $\phi \in [0, 2\pi]$ in $\mathbf{r}_\nu = (r_\nu, \theta, \phi)$ are sampled from uniform distributions over the respective intervals, employing existing symmetry. If the next-event type is a *Single Escape*, $r_\nu = R$ with certainty and no further steps are required. For the other event types, i.e. *Single Reaction* or bursting, the new radial distance r_ν is sampled from

$$r_\nu = P^{-1}_{S(\tau_\nu)}(\mathcal{R}_S) \tag{2.9}$$

with a uniform random number $\mathcal{R}_S \in [0, 1]$ and the cumulative conditional PDF

$$P_{S(\tau_\nu)}(r_\nu) = \frac{1}{S(\tau_\nu)} \int_0^{r_\nu} \int_0^{2\pi} \int_0^{\pi} p(r, \theta, \phi, \tau_\nu|\mathbf{r}_0) r^2 \sin(\theta) d\theta d\phi dr \quad . \tag{2.10}$$

If a *Single Reaction* event produces two particles from one, these are put at contact at the sampled position $\mathbf{r}_\nu$ with random spatial orientation. If it is a true decay event the particle is removed from the system together with its domain. Finally, when a *Single Reaction* induces a change the particle species from s_0 to s, the s_0 particle is removed and a new s-particle is created at $\mathbf{r}_\nu$. In any other event the particle is simply moved to $\mathbf{r}_\nu$.

[1] As a matter of course, using $1 - \mathcal{R}_e$ and $\mathcal{R}_e$ is equivalent if both are uniform random numbers from $[0, 1]$.

2.1.3 Pair domains

Sampling of next-event times for a *Pair* domain $\mathcal{D}_2$ follows the same principles as for *Singles*. However, here the two particles can react at contact, which creates an additional channel of exit from the domain and a new next-event type.

Let us denote by $p_2(\mathbf{r}_\mathrm{A}, \mathbf{r}_\mathrm{B}, t|\mathbf{r}_\mathrm{A0}, \mathbf{r}_\mathrm{B0})$ the PDF for the likelihood of finding two diffusing particles A and B initially located at positions $\mathbf{r}_\mathrm{A0}$ and $\mathbf{r}_\mathrm{B0}$ at $t = t_0$ at positions $\mathbf{r}_\mathrm{A}$ and $\mathbf{r}_\mathrm{B}$ at a later time t. The time-evolution of p_2 is governed by the SMOLUCHOWSKI equation:

$$\partial_\mathrm{t} p_2 = [D_\mathrm{A}\nabla_\mathrm{A}^2 + D_\mathrm{B}\nabla_\mathrm{B}^2]p_2 \tag{2.11}$$

Here D_A and D_B are the diffusion constants of particles A and B. As demonstrated later for a more general case, this problem can be simplified by transforming coordinates $\mathbf{r}_\mathrm{A}$ and $\mathbf{r}_\mathrm{B}$ to $\mathbf{r}$ and $\mathbf{R}$, where $\mathbf{r}$ is the interparticle vector and $\mathbf{R}$ the (weighted) center-of-mass of the particles. A separation ansatz $p_2 = p_\mathrm{r}(\mathbf{r})p_\mathrm{R}(\mathbf{R})$ then yields two separate, uncoupled diffusion equations for $\mathbf{r}$ and $\mathbf{R}$, which are equivalent to (2.11):

$$\partial_\mathrm{t} p_\mathrm{r} = D_\mathrm{r}\nabla_\mathrm{r}^2 p_\mathrm{r}\ , \qquad \partial_\mathrm{t} p_\mathrm{R} = D_\mathrm{R}\nabla_\mathrm{R}^2 p_\mathrm{R} \quad . \tag{2.12}$$

The constants D_r and D_R depend only on D_A and D_B. The uncoupling allows for the calculation of two Green's function solutions $p_\mathrm{r}(\mathbf{r}, t|\mathbf{r}_0)$ and $p_\mathrm{R}(\mathbf{R}, t|\mathbf{R}_0)$ on two subdomains $\mathcal{D}_\mathrm{r}$ and $\mathcal{D}_\mathrm{R}$ of $\mathcal{D}_2$, respectively, with boundary conditions adapted to the problem as described further below. $\mathcal{D}_\mathrm{r}$ and $\mathcal{D}_\mathrm{R}$ must be defined in a way that all possible positions constructed from sampled values of $\mathbf{r}$ and $\mathbf{R}$ remain within the protective domain $\mathcal{D}_2$. Figure 2.2A shows a valid definition of the subdomains for a (projected) spherical pair domain.

The Green's function p_R for the $\mathbf{R}$ diffusion is calculated in precisely the same way as the Green's function for the one-particle problem in *Single* domains, with an absorbing boundary condition $p_\mathrm{R}(\mathbf{R}, t) = 0$ for $\mathbf{R} \in \partial\mathcal{D}_\mathrm{R}$. This yields a next-event time τ_R for first-arrival of $\mathbf{R}$ to $\partial\mathcal{D}_\mathrm{R}$, called *Center of Mass Escape* or *CoM Escape*.

Reactions between A and B are modelled via a radiating boundary condition to p_r at the particle contact radius $\sigma = R_\mathrm{A} + R_\mathrm{B}$:

$$q_\sigma(t) \equiv \int_{\partial\mathcal{D}_\mathrm{r}^\sigma} -D\nabla_\mathbf{r} p_\mathrm{r}(\mathbf{r}, t|\mathbf{r}_0)d\mathbf{r} = k p_\mathrm{r}(|\mathbf{r}| = \sigma, t) \tag{2.13}$$

Here, k is the intrinsic particle reaction rate, which is the rate at which the particles react given that they are in contact, and $p_\mathrm{r}(|\mathbf{r}| = \sigma, t)$ is the probability that the particles are indeed at contact at time t. The integral on the left is the total probability (out)flux through the "contact surface" or inner boundary of the $\mathbf{r}$-subdomain, which is the set of all points at which A and B are in contact: $\partial\mathcal{D}_\mathrm{r}^\sigma = \{\mathbf{r}||\mathbf{r}| = \sigma\}$. At the outer boundary of the $\mathbf{r}$-subdomain $\partial\mathcal{D}_\mathrm{r}^a$ absorbing boundary conditions are imposed. The initial condition for this boundary value problem is set by the inital separation of the two particles, $p_\mathrm{r}(\mathbf{r}, t = 0|\mathbf{r}_0) = \delta(\mathbf{r} - (\mathbf{r}_\mathrm{B0} - \mathbf{r}_\mathrm{A0}))$. A tentative next-event time τ_r can be sampled from the survival probability $S_\mathrm{r}(t) = \int_{\mathcal{D}_\mathrm{r}} p_\mathrm{r}(\mathbf{r}, t|\mathbf{r}_0)d\mathbf{r}$ in the same way as before. With this, however, it remains undetermined by which boundary the particle escaped. To specify whether the exit from $\mathcal{D}_\mathrm{r}$ happens through the radiating (*Pair Reaction* event) or through the absorbing boundary (*IV Escape*[2]), the probability

[2] IV = interparticle vector

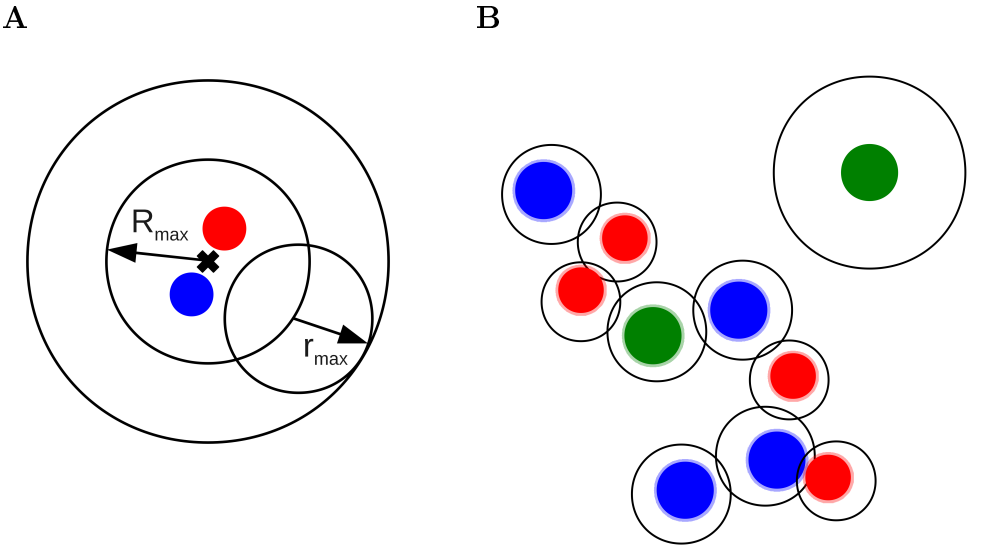

Figure 2.2: Pair and Multi domains in eGFRD. (A) Decomposition of a (projected) spherical *Pair* domain into subdomains for the center-of-mass vector $\mathbf{R}$ and the interparticle vector $\mathbf{r}$. (B) An exemplary *Multi* domain. Here we show the situation in which particles inside the *Multi* have been already propagated by earlier updates (and thus are offset with respect to the shells), but none of them reached its outer shell yet. Thin faint-color rings around the particles indicate their reaction volume. A blue and a red particle in the lower-right part of the Multi overlap with their reaction volumes and will attempt a reaction. Since enough space was available, the top-right green particle formed a regular *Single* domain.

fluxes through the boundaries at time τ_r are compared: If a uniformly distributed random number $\mathcal{R}_\mathrm{r} \in [0,1]$ is smaller than the fractional propensity

$$q_\mathrm{frac}(\tau_\mathrm{r}) = \frac{q_\sigma(\tau_\mathrm{r})}{q_\sigma(\tau_\mathrm{r}) + q_\mathrm{a}(\tau_\mathrm{r})} = \frac{q_\sigma(\tau_\mathrm{r})}{-\partial_\mathrm{t} S_\mathrm{r}(\tau_\mathrm{r})} \tag{2.14}$$

the next-event is a *Pair Reaction*; otherwise it is a *IV Escape*.

In general, particles A and B additionally can undergo monomolecular reactions, for which next-event times τ_A and τ_B are calculated in the same manner as for *Singles*. Thus, during *Pair* domain construction, altogether four next-event times τ_r, τ_R, τ_A, τ_B with different next-event types are determined. Since the four stochastic processes again are independent of each other, the tentative next-event time for the *Pair* domain is defined as:

$$\tau_{\mathcal{D}_2} = \min\left(\{\tau_\mathrm{r}, \tau_\mathrm{R}, \tau_\mathrm{A}, \tau_\mathrm{B}\}\right) \tag{2.15}$$

The precise procedure of sampling new positions for A and B at next-event time $\tau_{\mathcal{D}_2}$ depends on the type of the next event and the coordinate system in which the problem is considered. We present here the classical treatment for two interacting

particles in 3D, which employs spherical coordinates, for each possible event-type respectively:

- *Pair Reaction*: Here the CoM position $\mathbf{R}_\nu(\tau_\mathrm{r})$ is sampled in the same manner as the new position $\mathbf{r}_\nu(\tau < \tau_{\mathcal{D}_1})$ in *Singles*. A particle with the product species is created at $\mathbf{R}_\nu(\tau_\mathrm{r})$.

- *IV Escape*: In this case $|\mathbf{r}_\nu| = a$ with certainty, but the escape angle θ_ν yet remains undetermined. It is sampled from the propensity function for leaving the **r**-subdomain at the **r**-escape time τ_r through its outer boundary at an angle θ, given by

$$q_\mathrm{a}(\theta) = -\frac{a\sin(\theta)}{Q} D_\mathrm{r} \int_0^{2\pi} \left[\partial_\mathrm{r} p_\mathrm{r}(r,\theta,\phi,\tau_\mathrm{r}|\mathbf{r}_0)\right]_{\mathrm{r=a}} a d\phi \; .$$

  Here the normalization factor is the total flux through the outer boundary $Q = \int_0^\pi q_\mathrm{a}(\theta)d\theta$. The second angle $\phi_\nu \in [0, 2\pi]$ is drawn from a uniform distribution.

- *CoM Escape*: A new center-of-mass position $\mathbf{R}_\nu(\tau_\mathrm{R})$ is sampled as $\mathbf{r}_\nu(\tau_{\mathcal{D}_1})$ in the *Single*. To determine $\mathbf{r}_\nu(\tau_\mathrm{R})$, first a new radius r_ν is sampled from the conditional probability

$$\tilde{p}_\mathrm{r}(r,\tau_\mathrm{R}) \equiv \frac{r^2}{S_\mathrm{r}(\tau_\mathrm{R})} \int_0^\pi \int_0^{2\pi} p_\mathrm{r}(r,\theta,\phi,\tau_\mathrm{R}|\mathbf{r}_0)\sin(\theta) d\theta d\phi \; .$$

  Subsequently, a new angle θ_ν is sampled from the density $p_{\mathrm{r},\theta}(\theta, r_\nu, \tau_\mathrm{R}) \equiv \frac{r_\nu \sin(\theta)}{\tilde{p}_\mathrm{r}(r_\nu,\tau_\mathrm{R})} \int_0^{2\pi} p_\mathrm{r}(r_\nu,\theta,\phi,\tau_\mathrm{R}|\mathbf{r}_0)d\phi$ and $\phi_\nu \in [0, 2\pi]$ from the uniform distribution.

- *Monomolecular reaction* (of A)[3]: The new CoM position $\mathbf{R}_\nu(\tau_\mathrm{A})$ is sampled as in the case *Pair Reaction*, the new interparticle vector $\mathbf{r}_\nu(\tau_\mathrm{A})$ as in the case *CoM Escape*. From this we obtain $\mathbf{r}_{\mathrm{A},\nu}(\tau_\mathrm{A})$ and $\mathbf{r}_{\mathrm{B},\nu}(\tau_\mathrm{A})$. Particle B is simply moved to $\mathbf{r}_{\mathrm{B},\nu}(\tau_\mathrm{A})$, while A is treated as described for the monomolecular reactions in *Singles*.

[3] An identical procedure applies, with A and B interchanged, to the case in which B undergoes a monomolecular reaction.

2.1.4 Brownian Dynamics provides a fallback-system

The strength of eGFRD is that–due to the knowledge of the Green's function–detailed sampling of diffusive trajectories inside the domains can be omitted and particles are propagated with large jumps in time and space. This, however, comes at the cost of increased computational effort per update, because drawing times and positions from Green's functions is significantly more expensive than sampling of simple Gaussian displacements. Therefore eGFRD becomes more costly than Brownian Dynamics (BD) when particles get such crowded that the maximal size of protective domains becomes comparable to particle radii. This may be due to the presence of more than one other particle or other, static obstacles. In such situations, eGFRD seamlessly switches to a simulation mode in which particles are propagated by Brownian Dynamics within specialized domains, called *Multis*.

Multi domains

Whenever particle distances fall below a predefined threshold and regular domain types cannot be constructed, the algorithm prompts the construction of *Multi* domains, which can contain more than two particles. An exemplary *Multi* domain is shown in Figure 2.2B. *Multis* are composed of intersecting spherical shells with shell radii ρ_n proportional to particle radii R_n, i.e. $\rho_\mathrm{n} = \mu R_\mathrm{n}$, where the "multi-shell factor" $\mu > 1$ is a simulation parameter. Each *Multi* constitutes an autonomous BD simulator isolated from its surroundings. Within their shells, particles are propagated, one at a time, by sampling displacements $\Delta\mathbf{r}$ from the free Gaussian propagator with a fixed, sufficiently small timestep Δt that ensures $|\Delta\mathbf{r}| \ll \rho_\mathrm{n}$. Particle propagation continues until either one of the particles hits its surrounding shell or two overlapping particles react. Then, the *Multi* is broken apart and the new constellation is evaluated de novo, possibly resulting in *Multi* reconstruction. Particles that moved away sufficiently far from the particle crowd or obstacle at that moment reform *Single* domains and revert to propagation via Green's functions.

When and how *Multis* are constructed is explained in more detail in section 2.B.2 in the appendix.

Reactions in BD fulfill detailed balance

Particles that create overlaps within *Multis* are tested for reactions. Reaction events in BD mode are sampled such that detailed balance is obeyed. Let $\mathbf{r}_{12}$ be the interparticle vector of the two interacting particles. Detailed balance demands that, for any $\mathbf{r}_{12}$, the probability of the unbound configuration at distance $|\mathbf{r}_{12}|$ times the transition probability to move into the bound state from $\mathbf{r}_{12}$ equals the likelihood to be in the bound state times the probability of the inverse transition:

$$p_\mathrm{u}(\mathbf{r}_{12})\pi_{\mathrm{u}\to\mathrm{b}}(\mathbf{r}_{12}) = p_\mathrm{b}\pi_{\mathrm{b}\to\mathrm{u}}(\mathbf{r}_{12}) \tag{2.16}$$

The occupancy ratio $p_\mathrm{b}/p_\mathrm{u}(\mathbf{r}_{12}) = K_\mathrm{eq}$ is fixed by the equilibrium constant of the reaction and $\pi_{\mathrm{u}\to\mathrm{b}}(\mathbf{r}_{12})$ depends on algorithmic details of particle propagation. This leaves us with the task to prescribe a backward move in a way that $\pi_{\mathrm{b}\to\mathrm{u}}(\mathbf{r}_{12})$ obeys (2.16). Originally, eGFRD employed the Reaction Brownian Dynamics algorithm by

MORELLI and TEN WOLDE [60]. While this scheme yields excellent results for diffusing spheres in 3D, it proved troublesome to extend it to arbitrary dimensions and non-spherical objects. In recent eGFRD we therefore implemented a conceptually similar but more versatile scheme. Its key assumption is that reactive objects, be it other particles or static structures, are surrounded by a small "reaction volume" V^* within which the precise shape of the density $p_{\mathrm{u}}(\mathbf{r}_{12})$ may be ignored. Reaction attempts only occur within V^*, and at the inverse reaction the particle is placed uniformely back into V^*. The binding process is thus broken apart into a displacement and a reaction step. As in [60], it proves useful to rewrite the transition probabilities as a product of a proposal (i.e. move generation) density and (reaction) acceptance probability:

$$\begin{aligned}\pi_{\mathrm{u}\to\mathrm{b}}(\mathbf{r}_{12}) &= P^{\mathrm{gen}}_{\mathrm{u}\to\mathrm{V}^*}(\Delta t)P^{\mathrm{acc}}_{\mathrm{V}^*\to\mathrm{b}} \\ \pi_{\mathrm{b}\to\mathrm{u}}(\mathbf{r}_{12}) &= P^{\mathrm{gen}}_{\mathrm{V}^*\to\mathrm{u}}(\Delta t)P^{\mathrm{acc}}_{\mathrm{b}\to\mathrm{V}^*}\end{aligned} \tag{2.17}$$

Herein $P^{\mathrm{gen}}_{\mathrm{u}\to\mathrm{V}^*}(\Delta t)$ is the probability to move diffusively into the reaction volume V^* from a distance $\mathbf{r}_{12}$ in the unbound state within a time Δt, whereas $P^{\mathrm{gen}}_{\mathrm{V}^*\to\mathrm{u}}(\Delta t)$ is the probability of the inverse move. It can be shown that these probabilities only differ by a factor V^*: $P^{\mathrm{gen}}_{\mathrm{V}^*\to\mathrm{u}}(\Delta t) = V^* P^{\mathrm{gen}}_{\mathrm{u}\to\mathrm{V}^*}(\Delta t)$. Together with the assumption that unbinding occurs with Possonian statistics, i.e. $P^{\mathrm{acc}}_{\mathrm{b}\to\mathrm{V}^*} = k_{\mathrm{u}}\Delta t$, one finds that detailed balance is fulfilled when forward reaction attempts are accepted with a rate

$$P^{\mathrm{acc}}_{\mathrm{V}^*\to\mathrm{b}} = \frac{k_{\mathrm{b}}\Delta t}{V^*} \quad . \tag{2.18}$$

In practice V^* depends on the given situation and it is convenient to tune the magnitudes of specifically occuring reaction volumes via a global "reaction length" parameter δ. For two spherical particles with contact radius σ we have $V^* = \frac{4}{3}\pi\left((\sigma+\delta)^2 - \sigma^2\right)$. For the particle-surface interactions that we introduce later V^* is calculated similarly, taking into account the particular geometry of the contact region. This is described in more detail in [61].

The reaction length δ and the propagation time step Δt are set for each *Multi* domain individually, subject to the following two constraints:

$$D_{\max}\Delta t \leq (\phi R_{\min})^2 \tag{2.19}$$

$$\frac{k_{\mathrm{b,max}}\Delta t}{\delta} \leq P^{\mathrm{acc}}_{\max} \tag{2.20}$$

Here $D_{\max}$ is the maximal diffusion constant of a particle in the *Multi*, $R_{\min}$ the minimal particle radius, $k_{\mathrm{b,max}}$ the fastest intrinsic forward rate (divided by dimension-specific contact-surface factors) and $\phi \leq 1$ a tuneable step size fraction. The first requirement limits the maximal displacement within timestep Δt to a fraction of the smallest particle size; the second ensures that the acceptance probability remains bounded by a value ≤ 1 also for fast reactions. The standard choice in eGFRD is $P^{\mathrm{acc}}_{\max} = 0.01$ and $\delta = \phi R_{\min}$ with $\phi = 0.05 - 0.10$.

2.1.5 Practical aspects

On the practical level, additional attention has to be devoted to some further aspects. In particular, we were not concerned about details of creating protective domain shells given a certain constellation of surrounding shells. While it is clear that in principle one would like to size them up as much as possible, precisely because this makes it possible to make large jumps in time and space, in practice it turns out that this directive by itself may provoke unfavorable behavior that hampers efficiency. Specifically, a domain that is sized up to the boundary of a rather small neighboring domain is likely to be bursted shortly afterwards, when the small domain is updated; this forces domain reconstruction from scratch from almost the same situation as before, wasting computational effort. Moreover, while we explained in section 2.1.4 that it is advantageous to locally propagate particles by Brownian Dynamics when they get crowded, it is not a priori clear when precisely the transition between the two simulation modes should be done. We give a full account of measures that deal with these issues in section 2.B.2 in the appendix, where we present a detailed description of domain making rules in eGFRD.

Implementation

eGFRD is implemented with a core-system written in *C++* and a *Python*-based annex part. The core system is embedded into *Python* via *Boost.Python*. While the usage of *C++* at the core level ensures high computation efficiency, the attached *Python* interface provides a user-friendly scripting environment. eGFRD makes intense use of *GNU Scientific Library*, *Numpy*, *Scipy*, *Automake* and *GNU Libtool*. In later 2012 eGFRD surpassed the 150k linecount. The open-source code is stored in an online *git* repository accessible from the eGFRD website (http://gfrd.org).

Performance

eGFRD has demonstrated hitherto unmatched computational efficiency as a truly particle-based stochastic simulation environment in simulations of reacting hard spheres. It clearly outperforms classical Brownian Dynamics up to μM particle concentrations [39, 42], which is well within the biologically relevant regime. At higher particle densities BD becomes favorable for the reasons explained in section 2.1.4. For particles in a finite, constant 3D volume with periodic boundary conditions the CPU time scales as $N^{5/3}$ with the particle number N. For the extended simulator with the new features that we present in the forthcoming sections and chapters, detailed benchmarking remains yet to be performed.

2.2 Introducing 1D transport into eGFRD

In cells, 1D transport is common. There are two princpal types of 1D transport: diffusion on linear structures, an example of which is DNA sliding [62, 63, 64], and cytoskeletal active transport [65, 66]. In active transport, cargo such as proteins, vesicles or virus vectors, is transported via molecular motors on linear macropolymer tracks like microtubules and actin filaments. Molecular motors consist of a stalk domain that bind the cargo and two foot domains that can attach to the polymer track. There are two major classes of molecular motors: processive and non-processeive motors [67]. Processive motors can move preferentially into one direction in a walking-like fashion while remaining bound to the filament. This is achieved through an ATP-powered sequence of reactions that induce periodic allosteric changes of the motor structure, in a way that one foot remains bound to the track while the other one is first protruded towards and then anchored to a neighboring lattice site on the track. In spite of reaction reversibility, permanent consumption of ATP makes the forward-step reaction more probable than the backward-step. This way, a biased random walk of the motor towards a specific end of the linear track is created. Although non-processive motors also can change their confirmation upon binding to a filament, they are incapable of taking successive steps. Nevertheless, multiple groups of non-processive motors can create a step-like movement and drag cargo along the filament collectively. However, the resulting movement is much more irregular as compared to processive motors, with diffusion dominating over drift.

GFRD heavily relies on the availability of exact analytical solutions for the diffusion-reaction problem in simple geometries. Under this constraint, details like motor structure and filament curvature, which massively complicate mathematical calculations, have to be abandoned. In order to implement 1D transport into GFRD we therefore devised a minimal model of diffusive and active transport on linear tracks: Tracks are represented as thin, long cylinders with a reactive surface. Sliding proteins and motor-cargo complexes are assumed to be well-represented by perfectly spherical (single) particles. The biased 1D random walk is described by a modified diffusion equation that contains an additional drift term. These simplifications enables us to introduce (cylindrical) domains that produce next-event times for binding to and displacements on the cylinders, using the associated Green's functions.

In what follows, after introducing some new terminology, we first describe how we treat binding of particles from the cytosol to the reactive cylindrical structures and the reverse process. We then explain modelling of 1D movement of particles on the cylinders. The mathematical derivation of the required Green's functions is subject of the subsequent section 2.3.

2.2.1 Structures, surfaces and interactions

Here we briefly clarify the use of new terminology.

We will call static objects on which particles can exist "structures". This may be the 3D volume, called the "bulk" structure, or submanifolds of the 3D space, like cylinders and planes, referred to as "surfaces".

Further, we will distinguish between "reactions", i.e. the binding of particles to particles, and "interactions", which is the binding of particles to surfaces. Instant transfer of particles from one surface to another is called "transitions". Accordingly, in addition to the basic classification into *Singles* and *Pairs*, we distinguish between "*Interaction*" and "*Transition*" domains, in which, respectively, particles can bind to surfaces or jump from one surface to another. The four domain categories are not necessarily mutually exclusive: *Transitions* can be *Singles* or *Pairs*, whereas *Interactions* are always *Single* domains. For completeness, we refer to *Singles* that are not *Interactions* as "*Non-Interaction Singles*". Note that *Non-Interaction Singles* may also exist on surfaces.

A domain class tree illustrating the categorization of domain types, which also includes new domain types introduced in the next chapter, is shown in Figure S2.1 in appendix section 2.B.1.

2.2.2 Interactions with cylinders

Let us assume a situation in which a spherical particle that diffuses in 3D is close to a long cylinder with a reactive surface to which the particle can bind with an intrinsic forward rate k. To isolate the particle-surface association problem from the influence of surrounding particles and surfaces we construct a cylindrical protective domain, with an axis that coincides with the axis of the reactive surface and such that it contains only the proximate particle. A sketch of such a "*Cylindrical Surface Interaction*" domain is shown in Figure 2.3A. For the one-particle surface-binding problem an analytical solution can be readily obtained.

Diffusion of the particle within the cylindrical domain is described by the diffusion equation in cylindrical coordinates $\mathbf{r} = (r, \phi, z)$:

$$\partial_{\mathrm{t}} p(\mathbf{r}, t|\mathbf{r}_0) = D\nabla^2 p(\mathbf{r}, t|\mathbf{r}_0) = D\left[\frac{1}{r}\partial_{\mathrm{r}}\left(r\partial_{\mathrm{r}}\right) + \frac{1}{r^2}\partial_{\phi}^2 + \partial_{\mathrm{z}}^2\right] p(\mathbf{r}, t|\mathbf{r}_0) \tag{2.21}$$

Since here diffusion in the direction parallel to the cylinders and diffusion in the direction orthogonal to the cylinders are not correlated, the above 3D diffusion equation can be uncoupled into a 1D and 2D problem using a separation ansatz $p(\mathbf{r}, t|\mathbf{r}_0) = p_{\mathrm{r}}(r, \phi, t)p_{\mathrm{z}}(z, t)$. This yields:

$$\partial_{\mathrm{t}} p_{\mathrm{r}}(r, \phi, t) = D\left[\frac{1}{r}\partial_{\mathrm{r}}\left(r\partial_{\mathrm{r}}\right) + \frac{1}{r^2}\partial_{\phi}^2\right] p_{\mathrm{r}}(r, \phi, t) \tag{2.22}$$

$$\partial_{\mathrm{t}} p_{\mathrm{z}}(z) = D\partial_{\mathrm{z}}^2 p_{\mathrm{z}}(z, t) \tag{2.23}$$

Let the particle initially be located at $\mathbf{r}_0 = (r_0, \phi_0, z_0 = 0)$. Then we may write the initial condition as:

$$p(r, \phi, z, t = 0) = \delta(\mathbf{r} - \mathbf{r}_0) = \underbrace{\frac{1}{r}\delta(r - r_0)\delta(\phi - \phi_0)}_{p_{\mathrm{r}}(r,\phi,t=0)} \underbrace{\delta(z)}_{p_{\mathrm{z}}(z,t=0)} \tag{2.24}$$

To include the new domain into the existing eGFRD framework we have to compute the expected times of particle exit from the domain. Here exit can either happen

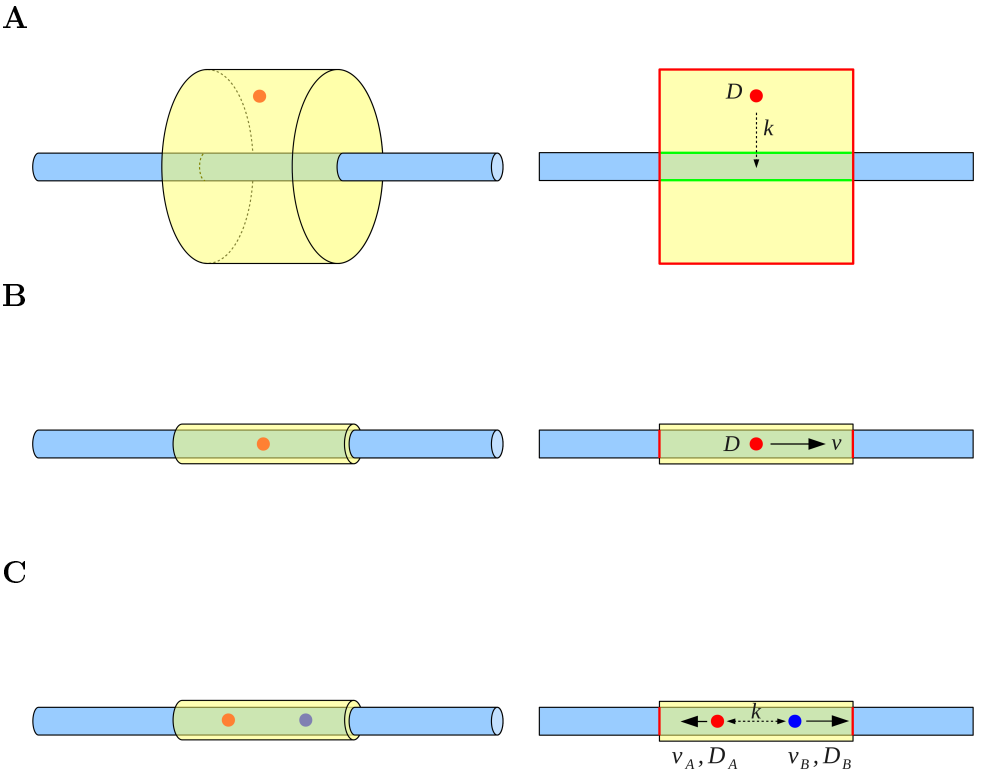

Figure 2.3: New protective domain types for interactions with and transport and reactions on 1D structures. (A) *Cylindrical Surface Interaction* domain; (B) *Cylindrical Surface Single* domain; (C) *Cylindrical Surface Pair* domain. Right panels show sections of 3D objects along the common cylinder axis. Absorbing boundaries are highlighted by red, radiative boundaries by green. Note that drift velocities (v, v_{A}, v_{B}) can be towards any cylinder end.

by hitting the absorbing outer boundary of the cylindrical domain or by reacting with the cylindrical structure enclosed by the domain. Let R_{D} and L be the radius and the length of the cylindrical domain, respectively, R_0 the radius of the reactive cylinder representing the filament and R the particle radius. Then the two aforementioned exit channels can be included into the model by imposing the following boundary conditions:

$$p_{\mathrm{z}}(-L/2,t) = 0, \qquad p_{\mathrm{z}}(+L/2,t) = 0 \tag{2.25}$$

$$p_{\mathrm{r}}(R_{\mathrm{D}},\phi,t) = 0 \tag{2.26}$$

$$2\pi\sigma D\partial_{\mathrm{r}}p_{\mathrm{r}}(r,\phi,t)\big|_{\mathrm{r}=\sigma} = kp_{\mathrm{r}}(|\mathbf{r}| = \sigma, t) \tag{2.27}$$

Here $\sigma = R + R_0$ is the contact radius, i.e. the radius of the cylindrical surface that

comprises all positions in which the particle is in contact with the reactive cylinder. $2\pi\sigma D\partial_r p_r(r,\phi,t)\big|_{r=\sigma}$ is the total outward probability flux in radial direction through the radiative boundary at $r=\sigma$ at time t, while $p_r(|\mathbf{r}|=\sigma,t)$ is the probability to be at contact with the reactive cylinder for the given t.

Clearly, the original 3D diffusion-reaction problem can be broken down into two problems that can be solved separately: Equations (2.22) with (2.26), (2.27) and the respective part of (2.24) constitute a boundary value problem for 2D diffusion of a point particle with a radiating boundary condition at $r=\sigma$ and an absorbing boundary condition at $r=R_D$. We present the Green's function for this problem in section 3.3.2. Equations (2.23) with (2.25) and the initial condition for p_z in (2.24) describe diffusion of a point particle in one dimension with two absorbing boundaries. The Green's function for this scenario follows as a special case of the Green's Function derived later in this chapter, as described in section 2.3.2.

2.2.3 Diffusion, drift and reactions on cylinders

Once a particle has bound to the cylindrical surface it can diffuse and drift along its axis and interact with other particles. To calculate next-event times for this scenario we again construct a protective domain around the particle. Here specifically we seek a domain that isolates cylinder-bound (1D) particles both from bulk (3D) particles and from other 1D particles simultaneously. While it certainly would be possible to take into account the finite thickness of the filament and rotational diffusion around the cylinder axis, we ignore these microscopic dynamics here; we argue that for most biological processes the dynamics at this molecular scale can be coarse-grained. Therefore we assume that the spherical particles in their bound state localize onto the axis of the cylinder. Then cylindrical domain geometry again is a natural choice, with a cylinder radius R_D equal to or greater than the particle radius. The length of the cylindrical domain is determined by the available free space, which in turn is limited by already present protective domains of other particles or the ends of the cylindrical surface if it is finite. In section 2.4 we describe in more detail how finite linear tracks are treated. Again we allow for one- (*Cylindrical Surface Single*, Fig. 2.3B) and two-particle domains (*Cylindrical Surface Pair*, Fig. 2.3C); the latter are formed when two cylinder-bound particles are close to each other. In addition, we introduce a special *Single* domain that encloses a reactive sink (*Cylindrical Surface Sink* domain, Fig. 2.5D) which may be used to model, for example, a reactive promoter site on DNA. More detail on the *Cylindrical Surface Sink* follows in sections 2.4 and 2.5.

The new domain types differ by their associated Green's functions. For the *Single* domains the Green's Function $p(x,t|x_0)$ is calculated from the diffusion-drift equation

$$\partial_t p(\mathbf{r},t|\mathbf{r}_0) = D\nabla^2 p(\mathbf{r},t|\mathbf{r}_0) - \mathbf{v}\nabla p(\mathbf{r},t|\mathbf{r}_0) \tag{2.28}$$

with two absorbing boundary conditions. Here the constant parameter $\mathbf{v}$ is the drift velocity of the particle and D the diffusion coefficient of the 1D diffusion process.

Similarly, in the *Pair* domains the spatio-temporal evolution of the combined probability density p_2 for two particles with diffusion constants D_A and D_B and (constant) drift velocities $\mathbf{v}_\mathrm{A}$ and $\mathbf{v}_\mathrm{B}$, respectively, may be described by the following SMOLUCHOWSKI equation [68, 39]:

$$\partial_\mathrm{t} p_2 = [D_\mathrm{A}\nabla_\mathrm{A}^2 + D_\mathrm{B}\nabla_\mathrm{B}^2 - \mathbf{v}_\mathrm{A}\nabla_\mathrm{A} - \mathbf{v}_\mathrm{B}\nabla_\mathrm{B}]p_2 \tag{2.29}$$

Herein $p_2 = p_2(\mathbf{r}_\mathrm{A}, \mathbf{r}_\mathrm{B}, t|\mathbf{r}_\mathrm{A0}, \mathbf{r}_\mathrm{B0})$ is the probability density function for the probability to find particle A at postion $\mathbf{r}_\mathrm{A}$ and particle B at $\mathbf{r}_\mathrm{B}$ at time t given that they started at $\mathbf{r}_\mathrm{A0}$ and $\mathbf{r}_\mathrm{B0}$ at $t = 0$. In section 2.3.1 we demonstrate that via an adequate coordinate transform we can decompose the combined diffusion-drift movement of both particles into two independent diffusion-drift processes for the center-of-mass and the interparticle vector, as already described in general for *Pairs* in section 2.1.3. This yields two equations of the same form as (2.28).

The fact that the required Green's function solutions follow from the same partial differential equation (2.28) facilitates further effort: In the following we will first derive the Green's function for the 1D diffusion-drift problem with one radiating and one absorbing boundary and then obtain the corresponding solution for the situation with two absorbing boundaries as a limit (section 2.3.2). The Green's function for the *Cylindrical Surface Sink* domain is treated as a special case in section 2.5.

2.2.4 Unbinding from cylinders

Unbinding from the cylindrical surfaces is treated in the same way as monomolecular reactions in standard eGFRD. A next-unbinding time τ_u is again sampled from an exponential distribution. Upon unbinding at time τ_u the cylindrical protective domain of the particle is bursted, i.e. particles are propagated until τ_m using the associated Green's function. After that, the unbinding particle is put at contact with the cylindrical surface at a random unbinding angle $\phi_\mathrm{u} \in [0, 2\pi]$. Of course, also monomolecular reactions that leave the particle on the cylinder or annihilate it are possible, and technically treated in the same way.

2.3 Green's functions for the diffusion-drift-reaction problem in 1D

In the following we derive Green's functions that are needed to sample next-event times for particles diffusing, drifting and interacting in 1D.

First we present the coordinate transform that is necessary to treat the two-particle problem.

2.3.1 Coordinate separation for the Smoluchowski equation

Starting from the SMOLUCHOWSKI equation [68] for two particles with diffusion coefficients D_A, D_B and drift velocities $\mathbf{v}_A$, $\mathbf{v}_B$

$$\partial_t p_2 = [D_A \nabla_A^2 + D_B \nabla_B^2 - \mathbf{v}_A \nabla_A - \mathbf{v}_B \nabla_B] p_2 \tag{2.30}$$

we define the interparticle vector $\mathbf{r}$ and the weighted center-of-mass vector $\mathbf{R}$ as follows:

$$\begin{aligned} \mathbf{r} &\equiv \mathbf{r}_B - \mathbf{r}_A \\ \mathbf{R} &\equiv \gamma \mathbf{r}_A + \delta \mathbf{r}_B \end{aligned} \tag{2.31}$$

γ and δ are constant coefficients that will be specified later.

In section 2.A of the appendix we show that operators ∇_A and ∇_B may be rewritten in terms of ∇_r and ∇_R as follows:

$$\begin{aligned} \nabla_A &= \gamma \nabla_R - \nabla_r \\ \nabla_B &= \delta \nabla_R + \nabla_r \end{aligned} \tag{2.32}$$

With the constraint $D_A \gamma = D_B \delta$, which causes mixed derivative terms $\sim \nabla_r \nabla_R$ to vanish, and after some intermediate steps one arrives at:

$$\begin{aligned} \partial_t p_2 =& \big[(D_A + D_B) \nabla_r^2 + (\gamma^2 D_A + \delta^2 D_B) \nabla_R^2 \\ & - \mathbf{v}_A (\gamma \nabla_R - \nabla_r) - \mathbf{v}_B (\delta \nabla_R + \nabla_r) \big] p_2 \\ =& \big[(D_A + D_B) \nabla_r^2 + (\gamma^2 D_A + \delta^2 D_B) \nabla_R^2 \\ & + (\mathbf{v}_A - \mathbf{v}_B) \nabla_r - (\gamma \mathbf{v}_A + \delta \mathbf{v}_B) \nabla_R \big] p_2 \end{aligned} \tag{2.33}$$

Via the separation ansatz $p_2 \equiv p_r p_R$ we can rewrite the above equation in terms of two diffusion-drift equations, one for $\mathbf{r}$ and one for $\mathbf{R}$, with diffusion and drift constants made up from the corresponding constants of the individual particles:

$$\begin{aligned} \partial_t p_r =& \big[\underbrace{(D_A + D_B)}_{D_r} \nabla_r^2 - \underbrace{(\mathbf{v}_B - \mathbf{v}_A)}_{\mathbf{v}_r} \nabla_r \big] \; p_r \\ \partial_t p_R =& \big[\underbrace{(\gamma^2 D_A + \delta^2 D_B)}_{D_R} \nabla_R^2 - \underbrace{(\gamma \mathbf{v}_A + \delta \mathbf{v}_B)}_{\mathbf{v}_R} \nabla_R \big] \; p_R \end{aligned} \tag{2.34}$$

The interpretation of the new drift constants is straightforward: $\mathbf{v}_\mathrm{r}$ describes the relative velocity of the particles (as in the case without diffusive motion) while $\mathbf{v}_\mathrm{R}$ is an effective weighted center-of-mass drift.

As explained in section 2.A, there is some freedom in choosing γ and δ as long as the constraint imposed above remains fulfilled. Here we make the same choice as in eGFRD:

$$\gamma = \frac{D_\mathrm{B}}{D_\mathrm{A} + D_\mathrm{B}}, \qquad \delta = \frac{D_\mathrm{A}}{D_\mathrm{A} + D_\mathrm{B}} \tag{2.35}$$

which implies:

$$D_\mathrm{R} = \frac{D_\mathrm{A} D_\mathrm{B}}{D_\mathrm{A} + D_\mathrm{B}}, \qquad \mathbf{v}_\mathrm{R} = \frac{D_\mathrm{B}\mathbf{v}_\mathrm{A} + D_\mathrm{A}\mathbf{v}_\mathrm{B}}{D_\mathrm{A} + D_\mathrm{B}} \tag{2.36}$$

With the definition of 1D structures and domains introduced in section 2.2 movement of the particles is restricted to a straight line. Then vectors $\mathbf{r}$, $\mathbf{R}$, $\mathbf{v}_\mathrm{r}$ and $\mathbf{v}_\mathrm{R}$ are collinear, and we can pass from the vector equation to a scalar equation.

2.3.2 Solution for the 1D-diffusion-reaction problem with drift with different boundary conditions

With the assumptions made in the previous section the 1D diffusion-drift equation takes the common form, where x stands for either the inter-particle distance r or the center-of-mass position R:

$$\partial_\mathrm{t} p_\mathrm{x} = \left[D_\mathrm{x}\partial_\mathrm{x}^2 - v_\mathrm{x}\partial_\mathrm{x}\right]\ p_\mathrm{x} \tag{PDE}$$

In both cases the initial condition is $p_\mathrm{x}(x, t_0 = 0) = \delta(x - x_0)$. In the following we will drop the index and simply use $p = p(x, t|x_0, t_0)$ to denote the Green's function. Following the standard treatment in eGFRD, we model chemical reactions between particles A and B on the cylinder by imposing a radiating boundary condition to r at particle contact, while the R-equation has to be solved subject to absorbing boundary conditions. For completeness, we will also give the solutions for the half-bounded problems.

To summarize, in the following we will derive the Green's function for (PDE) on an interval $[\sigma, a]$ of length $L = a - \sigma$ or on a one-sided interval $[\sigma, \infty)$, and the following boundary conditions, respecitvely:

- Rad-Abs: radiating left boundary at σ, absorbing right boundary at $a > \sigma$.
- Abs-Abs: absorbing left boundary at σ, absorbing right boundary at $a > \sigma$.
- Rad-Inf: radiating left boundary at σ, no right boundary.
- Abs-Inf: absorbing left boundary at σ, no right boundary.

The Green's Functions are used to derive the resulting survival probability $S(t|x_0, t_0) = \int_\mathrm{a}^{b \text{ or } \infty} p(x, t|x_0, t_0)dx$, the corresponding propensity function $\pi(t|x_0, t_0) = -\partial_\mathrm{t} S(t|x_0, t_0)$ and expressions for the transient boundary fluxes.

Free solution

It is easily verified that "free", i.e. unbounded, diffusion-drift equation (PDE) with initial condition $p(x, t = 0) = \delta(x - x_0)$ is solved by

$$p_{\text{free}}(x, t|x_0) = \frac{1}{\sqrt{4\pi Dt}} e^{-\frac{1}{4Dt}[(x-x_0)-vt]^2} \tag{2.37}$$

which describes a Gaussian distribution with a width that increases in time, centered around a mean value that moves with the drift velocity v.

Green's function for 1D-diffusion with drift, Rad-Abs case

We start with the most general of the four cases, with the perspective of deriving other cases as special limits.

The radiation boundary condition relates the probability flux $j(x = \sigma, t)$ at the radiating boundary to the intrinsic reaction rate k via:

$$j(x = \sigma, t) = -kp(x = \sigma, t) \tag{2.38}$$

Here the flux contains a contribution from diffusion and a contribution from the drift:

$$j(x, t) = -D\partial_{\text{x}} p(x, t) + vp(x, t) \tag{2.39}$$

The correct boundary condition for the boundary at $\sigma < a$ therefore is:

$$\begin{aligned} -D\partial_{\text{x}} p(x, t)\big|_{\text{x}=\sigma} + vp(\sigma, t) &= -kp(\sigma, t) \\ \Leftrightarrow \qquad \partial_{\text{x}} p(x, t)\big|_{\text{x}=\sigma} &= \frac{v + k}{D} p(\sigma, t) \end{aligned} \tag{BCr}$$

The minus sign on the right side of the equation is due to the fact that at the left boundary the flux out of the system is negative with respect to the x-axis.

The absorbing boundary at $x = a$ requires:

$$p(a, t) = 0 \qquad \forall t \tag{BCa}$$

Dedimensionalization

Before we attempt to solve the PDE with these boundary conditions it is convenient to perform a dedimensionalization. The natural length scale is given by the length $L = a - \sigma$ of the interval $[\sigma, a]$, while $T \equiv L^2/D$ defines a corresponding natural time scale. We thus rescale our variables via

$$\begin{aligned} \xi \equiv \frac{x - \sigma}{a - \sigma} = \frac{x - \sigma}{L}, \quad &\Rightarrow \partial_\xi \equiv L\partial_{\text{x}} \\ \tau \equiv \frac{t}{T} = \frac{Dt}{L^2}, \quad &\Rightarrow \partial_\tau \equiv T\partial_{\text{t}} = \frac{L^2}{D}\partial_{\text{t}} \end{aligned} \tag{2.40}$$

to obtain the following boundary value problem to solve:

$$\partial_\tau p(\xi,\tau) = \left[\partial_\xi^2 - \frac{vL}{D}\partial_\xi\right]\ p(\xi,\tau) \tag{PDE}$$

$$\partial_\xi p(\xi,\tau)\big|_{\xi=0} = \frac{(v+k)L}{D}p(0,\tau) \tag{BCr}$$

$$p(1,\tau) = 0 \tag{BCa}$$

$$p(\xi,\tau=0) = \frac{1}{L}\delta\left(\xi-\xi_0\right) \tag{IC}$$

The last equation represents the starting condition for a particle initially located at position $L\xi_0$ (or a pair having an initial separation $L\xi_0$), where for convenience we set $t_0 = 0 = \tau_0$. Note that we have to scale the delta function by $1/L$ because the integration norm scales as $d\xi = Ldx$.

Unfortunately the linear operator $\Lambda \equiv \left[\partial_\xi^2 - \frac{vL}{D}\partial_\xi\right]$ is non-Hermitian. Therefore we can not apply straightforward techniques like eigenfunction expansion to calculate the solution. As we will see, a simple transform can resolve this issue.

Simplifying the problem with the help of an integrating factor

The difficulties imposed by the non-Hermiticity of the operator can be overcome by introducing an integrating factor $\phi(\xi) \equiv e^{\frac{vL}{2D}\xi} = e^{\frac{\nu}{2}\xi}$ (depending explicitly on ξ)[4]. This technique was already used by Smoluchowski himself [69]. Multiplying (PDE) with $1/\phi(\xi) = e^{-\frac{\nu}{2}\xi}$ and completing the square yields ($\nu \equiv \frac{vL}{D}$):

$$\begin{aligned}
\partial_\tau\left[e^{-\frac{\nu}{2}\xi}p(\xi,\tau)\right] &= e^{-\frac{\nu}{2}\xi}\left[\partial_\xi^2 - \nu\partial_\xi\right]\ p(\xi,\tau) \\
&= \left[e^{-\frac{\nu}{2}\xi}\partial_\xi^2 - 2\frac{\nu}{2}e^{-\frac{\nu}{2}\xi}\partial_\xi + \frac{\nu^2}{4}e^{-\frac{\nu}{2}\xi}\right. \\
&\qquad\qquad \left. -\frac{\nu^2}{4}e^{-\frac{\nu}{2}\xi}\right]\ p(\xi,\tau) \\
&= \partial_\xi^2\left[e^{-\frac{\nu}{2}\xi}p(\xi,\tau)\right] - \frac{\nu^2}{4}e^{-\frac{\nu}{2}\xi}p(\xi,\tau)
\end{aligned} \tag{2.41}$$

Thus, by writing the solution with an ansatz

$$p(\xi,\tau) = \phi(\xi)\pi(\xi,\tau) = e^{\frac{\nu}{2}\xi}\pi(\xi,\tau) \tag{2.42}$$

which means defining a new function

$$\pi(\xi,\tau) \equiv e^{-\frac{\nu}{2}\xi}p(\xi,\tau) \tag{2.43}$$

equation (PDE) is equivalent to:

$$\partial_\tau\pi(\xi,\tau) = \partial_\xi^2\pi(\xi,\tau) - \frac{\nu^2}{4}\pi(\xi,\tau) \tag{2.44}$$

[4] Λ is non-Hermitian with respect to the usual Cartesian integration norm $d\xi$. However it is Hermitian with respect to the integration norm $d\phi = \frac{\nu}{2}e^{\frac{\nu}{2}\xi}d\xi$.

Alternatively, this can be seen by plugging the new ansatz for p into (PDE) and applying the operators accordingly.

As a next step, also the boundary conditions and the initial condition have to be transformed analogously to yield an equivalent of the whole problem. Clearly, $\pi(\xi,\tau) = 0$ whenever $p(\xi,\tau) = 0$. Thus, $\pi(\xi,\tau)$ fulfills the boundary condition at $\xi = 1$ trivially if $p(\xi,\tau)$ does so. Because of

$$\partial_\xi \pi(\xi,\tau) = \left[\partial_\xi e^{-\frac{\nu}{2}\xi}\right] p(\xi,\tau) + e^{-\frac{\nu}{2}\xi}\partial_\xi p(\xi,\tau)$$

we have

$$\begin{aligned}
\partial_\xi \pi(\xi,\tau)\big|_{\xi=0} &= -\frac{\nu}{2}p(0,\tau) + \left[e^{-\frac{\nu}{2}\xi}\partial_\xi p(\xi,\tau)\right]_{\xi=0} \\
&= -\frac{\nu}{2}p(0,\tau) + \frac{(v+k)L}{D}p(0,\tau) \\
&= \left[\frac{\nu}{2} + \frac{kL}{D}\right]\pi(0,\tau)
\end{aligned}$$

where in the last step we use $p(0,\tau) = \pi(0,\tau)$ and $\nu = \frac{vL}{D}$.

The initial condition becomes:

$$\pi(\xi,0) = e^{-\frac{\nu}{2}\xi}p(\xi,0) = e^{-\frac{\nu}{2}\xi}\frac{1}{L}\delta(\xi-\xi_0)$$

In the prefactor of the delta function ξ only takes values other than ξ_0 when the delta function is zero, so we can set $\xi = \xi_0$ here. This facilitates further calculations.

In summary, after multiplication with the integrating factor ϕ the initial problem for $p(\xi,\tau)$ is equivalent to the following problem for $\pi(\xi,\tau)$:

$$\partial_\tau \pi(\xi,\tau) = \left[\partial_\xi^2 - \frac{\nu^2}{4}\right]\pi(\xi,\tau) \tag{PDE}$$

$$\partial_\xi \pi(\xi,\tau)\big|_{\xi=0} = \left[\frac{\nu}{2} + \frac{kL}{D}\right]\pi(0,\tau) \tag{BCr}$$

$$\pi(1,\tau) = 0 \tag{BCa}$$

$$\pi(\xi,0) = e^{-\frac{\nu}{2}\xi_0}\frac{1}{L}\delta(\xi-\xi_0) \tag{IC}$$

This result reveals that the diffusion-drift problem is mathematically equivalent to a diffusion-decay problem with a slightly modified radiative boundary condition. The strategy now is to solve (PDE) for $\pi(\xi,t)$ and reconstruct the solution $p(\xi,t)$ afterwards using (2.42).

Solving the PDE via Laplace transform

Applying the Laplace transform by integrating $\int_0^\infty \pi(\xi,\tau)e^{-s\tau}d\tau \equiv \hat{\pi}(\xi,s)$ on both sides of (PDE) yields:

$$\begin{aligned}
& s\hat{\pi}(\xi,s) - e^{-\frac{\nu}{2}\xi_0}\frac{1}{L}\delta(\xi-\xi_0) = \left[\partial_\xi^2 - \frac{\nu^2}{4}\right]\hat{\pi}(\xi,s) \\
\Leftrightarrow \quad & \left[\partial_\xi^2 - \kappa^2\right]\hat{\pi}(\xi,s) = -\phi_0\delta(\xi-\xi_0)
\end{aligned} \tag{2.45}$$

where we abbreviate $\kappa^2 \equiv \frac{\nu^2}{4} + s \geq 0$ and $\phi_0 \equiv \frac{1}{L} e^{-\frac{\nu}{2}\xi_0} > 0$. According to transformation rules, the time derivative $\partial_\tau \pi(\xi, \tau)$ converts to $\hat{\pi}(\xi, s) - \pi(\xi, \tau = 0)$ in LAPLACE space.

To solve the transformed equation we first calculate the solution of the homogenous problem. This will be used to obtain two different specific solutions on the two parts of the underlying space separated by the delta peak, i.e. $[0, \xi_0]$ and $[\xi_0, 1]$, employing the boundary conditions and a continuity/discontinuity condition at $\xi = \xi_0$. The general solution to the homogenous problem $\partial_\xi^2 = \kappa^2 \hat{\pi}(\xi, s)$ can be written as $\hat{\pi}_\mathrm{h}(\xi, s) = \alpha \sinh(\kappa x) + \beta \cosh(\kappa x)$. We thus make an ansatz for each part of the interval $[0, 1]$ as follows:

$$\hat{\pi}(\xi, s) = \hat{\pi}_-(\xi, s) \equiv \alpha_- \sinh(\kappa\xi) + \beta_- \cosh(\kappa\xi) \qquad \text{for} \quad \xi < \xi_0 \tag{2.46}$$

$$\hat{\pi}(\xi, s) = \hat{\pi}_+(\xi, s) \equiv \alpha_+ \sinh(\kappa\xi) + \beta_+ \cosh(\kappa\xi) \qquad \text{for} \quad \xi > \xi_0 \tag{2.47}$$

with constant, yet arbitrary, real coefficients α_+, β_+ and α_-, β_-. Let us first apply the absorbing boundary condition at $\xi = 1$ to (2.47):

$$\hat{\pi}_+(1) = 0 \quad \Rightarrow \qquad \alpha_+ \sinh(\kappa) = -\beta_+ \cosh(\kappa) \tag{2.48}$$

where we neglect the unphysical solution $\alpha_+ = 0,\ \beta_+ = 0$.

Applying the transformed radiating boundary condition at $\xi = 0$ to (2.46) yields:

$$\begin{aligned}
&\partial_\xi \hat{\pi}_-(\xi, s)\big|_{\xi=0} = \underbrace{\left[\frac{\nu}{2} + \frac{kL}{D}\right]}_{\Omega} \hat{\pi}_-(0, s) \\
&\Leftrightarrow \left[\alpha_- \kappa \cosh(\kappa\xi) + \beta_- \kappa \sinh(\kappa\xi)\right]_{\xi=0} \\
&\qquad\qquad = \Omega \left[\alpha_- \sinh(\kappa\xi) + \beta_- \cosh(\kappa\xi)\right]_{\xi=0} \\
&\Leftrightarrow \kappa\alpha - = \Omega\beta_-
\end{aligned} \tag{2.49}$$

Reinsertion into (2.46) and (2.47) leads to:

$$\hat{\pi}_-(\xi, s) = \alpha_- \left(\sinh(\kappa\xi) + \frac{\kappa}{\Omega} \cosh(\kappa\xi)\right) \tag{2.50}$$

$$\hat{\pi}_+(\xi, s) = \alpha_+ \left(\sinh(\kappa\xi) - \tanh(\kappa) \cosh(\kappa\xi)\right) \tag{2.51}$$

In order to determine coefficients α_+ and α_- we, firstly, impose continuity of $\hat{\pi}(\xi, s)$ at $\xi = \xi_0$, i.e. $\hat{\pi}_-(\xi_0, s) = \hat{\pi}_+(\xi_0, s)$ for all s. Secondly, by integrating equation (2.45) over $[\xi_0 - \epsilon, \xi_0 + \epsilon]$ and taking the limit $\epsilon \to 0$, we obtain the following discontinuity condition for the left- and right-hand derivative $\partial_\xi \hat{\pi}(\xi, s)\big|_{\xi=\xi_0}$:

$$\begin{aligned}
&\int_{\xi_0-\epsilon}^{\xi_0+\epsilon} \left[\partial_\xi^2 \hat{\pi}(\xi, s) - \kappa^2 \hat{\pi}(\xi, s)\right] d\xi = -\int_{\xi_0-\epsilon}^{\xi_0+\epsilon} \phi_0 \delta(\xi - \xi_0) d\xi \qquad \Leftrightarrow \\
&\left[\partial_\xi \hat{\pi}(\xi, s)\big|_{\xi_0+\epsilon} - \partial_\xi \hat{\pi}(\xi, s)\big|_{\xi_0-\epsilon}\right] - \kappa^2 \left[\hat{\Pi}(\xi_0 + \epsilon, s) - \hat{\Pi}(\xi_0 - \epsilon, s)\right] = -\phi_0 \\
&\overset{\epsilon \to 0}{\Rightarrow} \qquad \partial_\xi \hat{\pi}_+(\xi, s)\big|_{\xi_0} - \partial_\xi \hat{\pi}_-(\xi, s)\big|_{\xi_0} = -\phi_0
\end{aligned} \tag{2.52}$$

The term $[\hat{\Pi}(\xi_0+\epsilon,s)-\hat{\Pi}(\xi_0-\epsilon,s)]$ vanishes for $\epsilon\to 0$ because continuity of $\hat{\pi}(\xi,s)$ at $\xi=\xi_0$ implies continuity of the stem function $\hat{\Pi}(\xi,s)=\int\hat{\pi}(\xi,s)d\xi$ at this point.

Applying the two additional constraints to (2.50) and (2.51) determines, after some algebraic steps, the coefficients α_- and α_+:

$$\begin{aligned}\alpha_- &= \frac{-\phi_0}{\kappa\left(\frac{\kappa}{\Omega}+\tanh(\kappa)\right)}\left(\sinh(\kappa\xi_0)-\tanh(\kappa)\cosh(\kappa\xi_0)\right)\\ \alpha_+ &= \frac{-\phi_0}{\kappa\left(\frac{\kappa}{\Omega}+\tanh(\kappa)\right)}\left(\sinh(\kappa\xi_0)+\frac{\kappa}{\Omega}\cosh(\kappa\xi_0)\right)\end{aligned} \tag{2.53}$$

Hence,

$$\begin{aligned}\hat{\pi}_-(\xi,s) &= \frac{-\phi_0}{\kappa\left(\frac{\kappa}{\Omega}+\tanh(\kappa)\right)}\times\\ &\qquad\left(\sinh(\kappa\xi)+\frac{\kappa}{\Omega}\cosh(\kappa\xi)\right)\left(\sinh(\kappa\xi_0)-\tanh(\kappa)\cosh(\kappa\xi_0)\right)\\ \hat{\pi}_+(\xi,s) &= \frac{-\phi_0}{\kappa\left(\frac{\kappa}{\Omega}+\tanh(\kappa)\right)}\times\\ &\qquad\left(\sinh(\kappa\xi_0)+\frac{\kappa}{\Omega}\cosh(\kappa\xi_0)\right)\left(\sinh(\kappa\xi)-\tanh(\kappa)\cosh(\kappa\xi)\right)\end{aligned} \tag{2.54}$$

or, after multiplying numerator and denominator by $\cosh(\kappa)$:

$$\begin{aligned}&\hat{\pi}_-(\xi,s) =\\ &\quad\frac{\phi_0}{\kappa}\frac{\left(\sinh(\kappa\xi)+\frac{\kappa}{\Omega}\cosh(\kappa\xi)\right)\left(\sinh(\kappa)\cosh(\kappa\xi_0)-\cosh(\kappa)\sinh(\kappa\xi_0)\right)}{\sinh(\kappa)+\frac{\kappa}{\Omega}\cosh(\kappa)}\\ &\hat{\pi}_+(\xi,s) =\\ &\quad\frac{\phi_0}{\kappa}\frac{\left(\sinh(\kappa\xi_0)+\frac{\kappa}{\Omega}\cosh(\kappa\xi_0)\right)\left(\sinh(\kappa)\cosh(\kappa\xi)-\cosh(\kappa)\sinh(\kappa\xi)\right)}{\sinh(\kappa)+\frac{\kappa}{\Omega}\cosh(\kappa)}\end{aligned} \tag{2.55}$$

Here we shall not forget that $\kappa=\kappa(s)=\sqrt{s+\frac{\nu^2}{4}}$.

With this we have determined unique solutions to the diffusion-drift-reaction problem for the left ($\xi\le\xi_0$) and right ($\xi\ge\xi_0$) part of the spatial domain in Laplace space. Now we can attempt the back transform to the time domain, where we will find that the solution becomes symmetric in ξ and ξ_0 again.

Inverse Laplace transform via residue formula

Having $\hat{\pi}(\xi,s)$ we can obtain the corresponding function in the time domain via the Bromwich / Fourier-Mellin integral:

$$\pi(\xi,t)=\mathcal{L}^{-1}\left[\hat{\pi}(\xi,z)\right]=\frac{1}{2\pi i}\lim_{\mathrm{T}\to\infty}\int_{\gamma-\mathrm{iT}}^{\gamma+iT}\hat{\pi}(\xi,z)e^{zt}dz \tag{2.56}$$

Herein $\hat{\pi}(\xi, z)$ is the extension of $\hat{\pi}(\xi, s)$ to the complex plane. The integration has to be performed on a line perpendicular to the real axis at the positive real value γ, which must be greater than the real part of any singularity of the complex function $\hat{\pi}(\xi, z)$. Usually this is a daunting task. It is simplified a lot if $\hat{\pi}(\xi, z)$ is a holomorphic function. In that case we can apply residue calculus to compute the line integral via a contour integral. To that purpose we close the line path from $\gamma - iT$ to $\gamma + iT$ by a half-circle in the space left to it ($\{z|\mathrm{Re}(z) \leq \gamma\}$) to obtain contour $\gamma'(T)$. In the limit $T \to \infty$ the half-circle contribution vanishes, i.e. $\lim_{\mathrm{T}\to\infty} \oint_{\gamma'(\mathrm{T})} \hat{\pi}(\xi, z)dz = \lim_{\mathrm{T}\to\infty} \int_{\gamma-\mathrm{iT}}^{\gamma+iT} \hat{\pi}(\xi, z)dz$. The residue formula states that the integral of $\hat{\pi}(\xi, z)$ along the contour is equal to the sum of residues at the singularities of $\hat{\pi}(\xi, z)$ enclosed by the contour times $2\pi i$. Thus, if all singularities of $\hat{\pi}(\xi, z)$ are to the left of γ, the inverse LAPLACE transform can be calculated as:

$$\pi(\xi, t) = \frac{1}{2\pi i} \lim_{\mathrm{T}\to\infty} \oint_{\gamma'(\mathrm{T})} \hat{\pi}(\xi, z)e^{zt}dz = \sum_{\mathrm{n}} \mathrm{Res}_{\hat{\pi}(\xi,\mathrm{z})\mathrm{e}^{\mathrm{zt}}}(z_{\mathrm{n}}) \tag{2.57}$$

Since $\hat{\pi}_-(\xi, s)$ and $\hat{\pi}_+(\xi, s)$ only differ by the fact that ξ and ξ_0 are interchanged it is sufficient to carry out the inverse transform for $\hat{\pi}_+(\xi, s)$ and obtain $\pi_-(\xi, t)$ by substituting $\xi \leftrightarrow \xi_0$.

As a first step we reinsert $\kappa = \sqrt{s + \frac{\nu^2}{4}}$ and substitute $s = z - \frac{\nu^2}{4}$ in $\hat{\pi}_+(\xi, s)$ where z is a complex variable now:

$$\hat{\pi}_+(\xi, z) = \frac{\phi_0}{\sqrt{z}} \frac{\left(\sinh(\xi_0\sqrt{z}) + \frac{1}{\Omega}\sqrt{z}\cosh(\xi_0\sqrt{z})\right)}{\sinh(\sqrt{z}) + \frac{1}{\Omega}\sqrt{z}\cosh(\sqrt{z})} \times \\ \left(\sinh(\sqrt{z})\cosh(\xi\sqrt{z}) - \cosh(\sqrt{z})\sinh(\xi\sqrt{z})\right) \tag{2.58}$$

Later, instead of reinserting $z = s + \frac{\nu^2}{4}$, we will apply the standard LAPLACE-inversion rule $\mathcal{L}^{-1}[\hat{f}(s + c)] = e^{-ct}f(t)$ for $c = const.$

The fact that $\hat{\pi}_+(\xi, z)$ contains $\sqrt{z}$ which is non-holomorphic on the negative real branch recommends testing holomorphicity of the function. By TAYLOR-expanding the $\sinh(const \cdot \sqrt{z})$ and $\cosh(const \cdot \sqrt{z})$ functions one can show that $\hat{\pi}_+(\xi, z)$ can be written as a sum over purely integer powers z^n and thus is indeed a holomorphic (even entire) function. Its complex roots z_{n} are found by setting the denominator to zero, which yields:

$$\tanh(\sqrt{z_{\mathrm{n}}}) = -\frac{1}{\Omega}\sqrt{z_{\mathrm{n}}} \tag{2.59}$$

It can be shown that all z_{n} lie on the negative real axis and that there is no singularity at $z = 0$. Since $\hat{\pi}_+(\xi, z)$ can be written as $\hat{\pi}_+(\xi, z) = g(z)/h(z)$ with functions $g(z)$ and $h(z)$ that are holomorphic in the neighborhood of each z_{n}, we may calculate the residue of $\hat{\pi}_+(\xi, z)$ at z_{n} via the well-known formula $\mathrm{Res}_{\hat{\pi}_+(\xi,\mathrm{z})\mathrm{e}^{\mathrm{zt}}}(z_{\mathrm{n}}) = g(z_{\mathrm{n}})/h'(z_{\mathrm{n}})$. Here we find, with $h(z) = \sinh(\sqrt{z}) + \frac{1}{\Omega}\sqrt{z}\cosh(\sqrt{z})$:

$$h'(z_{\mathrm{n}}) = \frac{1}{2\sqrt{z_{\mathrm{n}}}} \left[\left(1 + \frac{1}{\Omega} - \frac{z_{\mathrm{n}}}{\Omega^2}\right)\cosh(\sqrt{z_{\mathrm{n}}})\right] \tag{2.60}$$

In the next step we additionally substitute the square roots via $\sqrt{z_\mathrm{n}} \equiv \pm i\zeta_\mathrm{n}$ with $\zeta_\mathrm{n} \in \mathbb{R}^+$. Taking into account $\sinh(\pm ix) = \pm\sin(x)$ and $\cosh(\pm ix) = \cos(x)$ and cancelling multiplicative minus signs, the solution in the time domain as a sum of residues reads:

$$\begin{aligned}
\pi_+(\xi,\xi_0,t) &= \sum_\mathrm{n} \mathrm{Res}_{\hat{\pi}_+(\xi,\mathrm{z})e^{\mathrm{z}t}}(z_\mathrm{n}) \\
&= e^{-\frac{\nu^2}{4}t} \cdot 2\phi_0 \sum_\mathrm{n} e^{z_\mathrm{n}t} \frac{\sinh(\xi z_\mathrm{n}^{\frac{1}{2}}) + \frac{z_\mathrm{n}^{\frac{1}{2}}}{\Omega}\cosh(\xi z_\mathrm{n}^{\frac{1}{2}})}{\left(1+\frac{1}{\Omega}-\frac{z_\mathrm{n}}{\Omega^2}\right)\cosh(z_\mathrm{n}^{\frac{1}{2}})} \\
&\qquad \times \left(\sinh(z_\mathrm{n}^{\frac{1}{2}})\cosh(\xi_0 z_\mathrm{n}^{\frac{1}{2}}) - \cosh(z_\mathrm{n}^{\frac{1}{2}})\sinh(\xi_0 z_\mathrm{n}^{\frac{1}{2}})\right) \\
&= -\frac{2}{L} e^{-\frac{\nu^2}{4}t - \frac{\nu}{2}\xi_0} \cdot \sum_\mathrm{n} e^{-\zeta_\mathrm{n}^2 t} \frac{\sin(\xi\zeta_\mathrm{n}) + \frac{\zeta_\mathrm{n}}{\Omega}\cos(\xi\zeta_\mathrm{n})}{\left(1+\frac{1}{\Omega}+\frac{\zeta_\mathrm{n}^2}{\Omega^2}\right)\cos(\zeta_\mathrm{n})} \\
&\qquad \times \left(\sin(\zeta_\mathrm{n})\cos(\xi_0\zeta_\mathrm{n}) - \cos(\zeta_\mathrm{n})\sin(\xi_0\zeta_\mathrm{n})\right)
\end{aligned} \tag{2.61}$$

where the n-summation goes over the (positive) roots of the implicit equation

$$\tanh(\sqrt{z_\mathrm{n}}) = -\frac{1}{\Omega}\sqrt{z_\mathrm{n}} \quad \Leftrightarrow \quad \tan(\zeta_\mathrm{n}) = -\frac{1}{\Omega}\zeta_\mathrm{n} \tag{2.62}$$

with $\Omega = \frac{\nu}{2} + \frac{kL}{D} = \left(\frac{v}{2}+k\right)\frac{L}{D}$. Using the root equation (2.62) we can further simplify

$$\begin{aligned}
&\frac{\left(\sin(\zeta_\mathrm{n})\cos(\xi_0\zeta_\mathrm{n}) - \cos(\zeta_\mathrm{n})\sin(\xi_0\zeta_\mathrm{n})\right)}{\cos(\zeta_\mathrm{n})} = \\
&\qquad \tan(\zeta_\mathrm{n})\cos(\xi_0\zeta_\mathrm{n}) - \sin(\xi_0\zeta_\mathrm{n}) = -\left(\sin(\xi_0\zeta_\mathrm{n}) + \frac{\zeta_\mathrm{n}}{\Omega}\cos(\xi_0\zeta_\mathrm{n})\right)
\end{aligned} \tag{2.63}$$

and realize that the denominator of the summation terms in the time domain is completely symmetric in ξ and ξ_0. Hence, the solution in the time domain is invariant to interchanging ξ and ξ_0. After taking into account the integrating factor via $p(\xi,\xi_0,t) = e^{\frac{\nu}{2}\xi}\pi(\xi,\xi_0,t)$ and reverting dedimensionalization we can write the final solution for both sides of the spatial domain as:

$$p_\mathrm{RA}(x,x_0,t) \equiv$$

$$p(x,x_0,t) = \frac{2}{L} e^{\frac{v}{2D}(x-x_0) - \frac{v^2}{4D}t} \sum_\mathrm{n} e^{\frac{-\zeta_\mathrm{n}^2 Dt}{L^2}} \frac{F_\mathrm{n}(x)F_\mathrm{n}(x_0)}{\Omega^2+\Omega+\zeta_\mathrm{n}^2} \tag{2.64}$$

with

$$F_\mathrm{n}(x) \equiv \Omega\sin(\zeta_\mathrm{n}\frac{x-\sigma}{L}) + \zeta_\mathrm{n}\cos(\zeta_\mathrm{n}\frac{x-\sigma}{L}) \tag{2.65}$$

$$\Omega = \left(\frac{v}{2}+k\right)\frac{L}{D} \qquad \text{and} \tag{2.66}$$

$$\zeta_\mathrm{n} \quad \text{positive roots of} \qquad \tan(\zeta_\mathrm{n}) = -\frac{1}{\Omega}\zeta_\mathrm{n} \tag{2.67}$$

It can be easily verified that this function fulfills the imposed boundary conditions. Also the initial condition at $t = 0$ is recovered, which can be seen by expanding the delta function into the orthogonal functions $F_{\mathrm{n}}(x)$ and utilizing the straightforwardly proven orthogonality relation:

$$\int_{\sigma}^{a} F_{\mathrm{n}}(x)F_{\mathrm{m}}(x)dx = \begin{cases} \frac{L}{2}\left(\zeta_{\mathrm{n}}^2 + \Omega^2 + \Omega\right) & \text{for} \quad n = m \\ 0 & \text{for} \quad n \neq m \end{cases} \tag{2.68}$$

In the limit $v \to 0$ the solution reproduces the well-known solution for the case without drift, which can be found in [57, 14.3II, p. 360]. To verify this, set $\zeta_{\mathrm{n}} = \alpha_{\mathrm{n}} L$ in (2.64) and $k_1 = 1$, $k_2 = 0$, $h_1 = \frac{k}{D}$, $h_2 = 1$ in the reference formula.

Exemplary time evolution plots of $p_{\mathrm{RA}}(x, x_0, t)$ are shown in Figure 2.4 for different values of diffusion coefficient D, drift velocity v and intrinsic reaction rate k.

Green's function for 1D-diffusion with drift, Abs-Abs case

From (2.64) we can easily obtain the Green's function for 1D-diffusion with drift on a finite domain with two absorbing boundaries by taking the limit $k \to \infty$. The originally radiating boundary condition at $x = \sigma$ (BCr) then becomes

$$p(\sigma, t) = \frac{D\partial_{\mathrm{x}} p(x,t)\big|_{\mathrm{x}=\sigma} - v p(\sigma, t)}{k} \underset{k\to\infty}{\longrightarrow} 0 \quad . \tag{2.69}$$

First notice that because of $\Omega = \left(\frac{v}{2} + k\right)\frac{L}{D} \underset{k\to\infty}{\longrightarrow} 0$ the root equation (2.67) in the limit $k \to \infty$ reads:

$$\begin{aligned} &\tan(\zeta_{\mathrm{n}}) = -\frac{1}{\Omega}\zeta_{\mathrm{n}} \underset{k\to\infty}{\longrightarrow} 0 \\ &\Rightarrow \quad \zeta_{\mathrm{n}} = n\pi, \quad n \in \mathbb{N} \quad \text{for} \quad k \to \infty \end{aligned} \tag{2.70}$$

To obtain the limit of (2.64) we multiply the numerator and denominator of the summation terms by $1/k^2$. Because of

$$\frac{\Omega}{k} = \left(1 + \frac{v}{2k}\right)\frac{L}{D} \underset{k\to\infty}{\longrightarrow} \frac{L}{D} \tag{2.71}$$

we have

$$\frac{\Omega}{k}\sin\left(\zeta_{\mathrm{n}}\frac{x-\sigma}{L}\right) + \frac{\zeta_{\mathrm{n}}}{k}\cos\left(\zeta_{\mathrm{n}}\frac{x-\sigma}{L}\right) \underset{k\to\infty}{\longrightarrow} \frac{L}{D}\sin\left(\zeta_{\mathrm{n}}\frac{x-\sigma}{L}\right) \tag{2.72}$$

$$\frac{\Omega^2}{k^2} + \underbrace{\frac{\Omega}{k^2} + \frac{\zeta_{\mathrm{n}}^2}{k^2}}_{\to 0} \underset{k\to\infty}{\longrightarrow} \frac{L^2}{D^2} \tag{2.73}$$

and therefore:

$$\begin{aligned} &p_{\mathrm{AA}}(x, x_0, t) = p_{\mathrm{RA}}(x, x_0, t)\big|_{\mathrm{k}\to\infty} \\ &= \frac{2}{L} e^{\frac{v}{2D}(x-x_0) - \frac{v^2}{4D}t} \sum_{\mathrm{n}} e^{-\left(\frac{n\pi}{L^2}\right)^2 Dt} \sin\left(n\pi\frac{x-\sigma}{L}\right)\sin\left(n\pi\frac{x_0-\sigma}{L}\right) \end{aligned} \tag{2.74}$$

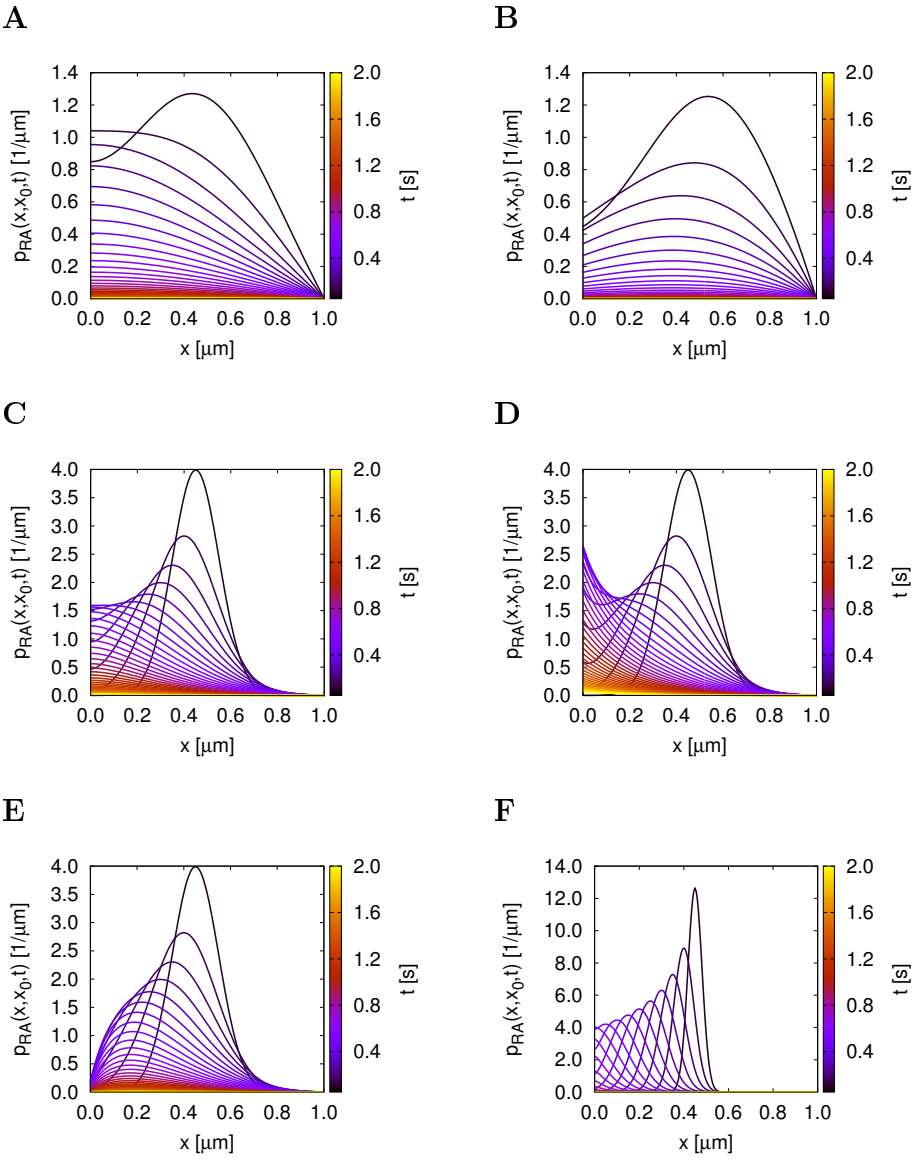

Figure 2.4: Green's function for the 1D diffusion-drift problem with radiating ($x = 0$) and absorbing ($x = 1$) boundary. (A) $D = 1.0$, $v = -1.0$, $k = |v|$; (B) $D = 1.0$, $v = +1.0$, $k = v$; (C) $D = 0.1$, $v = -1.0$, $k = |v|$; (D) $D = 0.1$, $v = -1.0$, $k = \frac{|v|}{2}$; (E) $D = 0.1$, $v = -1.0$, $k = 10|v|$; (F) $D = 0.01$, $v = -1.0$, $k = |v|$. Values are in $[\frac{\mu m^{(2)}}{s}]$. $x_0 = 0.5$ μm.

Green's function for 1D-diffusion with drift, Rad-Inf case

For completeness, we also mention here the Green's functions for the corresponding half-bounded problems. A solution for the case with only one radiating boundary at $x = 0$ and constant drift was already published by Lamm and Schulten [70] and reads:

$$\begin{aligned} & p_{\mathrm{R}\infty}(x,t|x_0,t=0) \\ &= \frac{1}{\sqrt{4\pi Dt}}\left(e^{-\frac{(x-x_0-vt)^2}{4Dt}} + e^{-\frac{vx_0}{D}}e^{-\frac{(x+x_0-vt)^2}{4Dt}}\right) \\ &\quad - \frac{v/2+k}{D}e^{\frac{vx_0}{D}}e^{\frac{k}{D}[(x+x_0)+(k+v)t]}\operatorname{erfc}\left(\frac{x+x_0}{\sqrt{4Dt}} + \frac{v/2+k}{D}\sqrt{Dt}\right) \end{aligned} \tag{2.75}$$

Green's function for 1D-diffusion with drift, Abs-Inf case

For the situation with only one absorbing boundary at $x = a \geq 0$ the Green's function for the 1D-diffusion-drift problem can be straightforwardly obtained via the method of images: Since any linear combination of the free solution $p_{\mathrm{free}}(x,t|x_0)$ fulfills the diffusion-drift equation, we can easily construct a solution $p_{\mathrm{A}\infty}(x,t|x_0)$ that will obey $p_{\mathrm{A}\infty}(a,t|x_0) = 0\ \forall t$ by subtracting from the free solution the antisymmetric solution for a particle starting from a distance $x_0 - a$ to the left of the boundary and with inverted drift $v \to -v$:

$$\begin{aligned} p_{\mathrm{A}\infty}(x,t|x_0) &= p_{\mathrm{free,v_+}}(x,t|x_0) - p_{\mathrm{free,v_-}}(x,t|a-(x_0-a)) \\ &= \frac{1}{\sqrt{4\pi Dt}}\left(e^{-\frac{1}{4Dt}[(x-x_0)-vt]^2} - e^{-\frac{1}{4Dt}[(x-2a+x_0)+vt]^2}\right) \end{aligned} \tag{2.76}$$

We verified that the above solution is equivalent to the solution for this problem calculated explicitly by applying the boundary conditions in Laplace space and inverting via the Residue formula, following the workflow described in section 2.3.2.

Survival probabilities

The survival probability is calculated by integration of the Green's function over the whole interval on which it is defined:

$$S(t) = \int_{\mathrm{a}}^{b} p(x,t|x_0)dx \tag{2.77}$$

For the half-bounded solutions $b = \infty$. The cumulative distribution function $P(x,t|x_0) = \int_{\mathrm{a}}^{x} p(x',t|x_0)dx'$ is needed besides $S(t)$ to sample positions at next-event times τ_ν. It is therefore convenient to first calculate $P(x,t|x_0)$ and then $S(t) = P(b,t|x_0)$ as a special case.

The Green's functions presented in this section all have the the form

$$p(x,t|x_0) = C_0 e^{\frac{v(x-x_0)}{2D}} \sum_{\mathrm{n}} c_{\mathrm{n}} f_{\mathrm{n}}(x) \tag{2.78}$$

where C_0 and c_n do not depend on x and $f_\mathrm{n}(x)$ are either trigonometric or GAUSS functions. To calculate $P(x,t|x_0)$ the integration is most conveniently performed term-wise, i.e. by computing $\int_\mathrm{a}^x e^{\frac{v(x'-x_0)}{2D}} f_\mathrm{n}(x')dx'$ with the help of partial integration and reassembling the sum. Differentiation of the survival probability gives the propensity function $q(t) \equiv -\partial_\mathrm{t} S(t)$. These are all straightforward calculations and therefore omitted here.

Boundary fluxes

With drift $v \neq 0$ the probability flux at position $x = x'$ is calculated from the Green's function $p(x,t|x_0)$ as follows:

$$q_{\mathrm{x}'}(t) = -D\partial_\mathrm{x} p(x,t|x_0)\big|_{\mathrm{x}=\mathrm{x}'} + vp(x',t|x_0) \tag{2.79}$$

Note that for an absorbing boundary at $x' = a$ we have $p(a,t|x_0) = 0$ and the drift-dependent term vanishes.

For a radiating boundary at $x' = \sigma$ with intrinsic reaction rate k it is more convenient to calculate the flux directly from

$$q_\sigma(t) = kp(\sigma,t|x_0) \tag{2.80}$$

which equals (2.79) with $x' = \sigma$ by construction of the problem.

For the Green's functions introduced in this chapter these expressions are again easily calculated and therefore not shown here. A complete collection of the surivival probabilities, cumulative distribution functions and boundary fluxes for all Green's functions presented in this chapter is available as part of the eGFRD technical documentation.

2.4 Finite cylindrical structures

Throughout this chapter until now we have assumed an infinite length for the cylindrical structures that particles interact with and are transported on. In many applications, however, we seek to study systems with finite 1D tracks, such as microtubules that canalize transported cargo to one of their ends preferentially, where it may unbind at a certain rate. Moreover, particles can behave differently after reaching the ends of microtubules by, for example, forming tip clusters [71, 72].

In order to include these features into eGFRD we introduce a new structure type, the disk structure, which is used to mark a special interaction site on a 1D cylindrical structure. A disk may be placed at the ends of a cylindrical structure of finite length to model reactive tip sites, or in any other place on the cylinder to model a point of interaction, e.g. a transcription-factor binding pocket on DNA. Within our framework a disk located at the end of a cylindrical structure is called a "cap", a disk located in between the ends a "sink". Particles on disks are immobilized. We allow particles on the cylinder to bind with a certain affinity both to disk structures and to particles already immobilized on caps. Unbinding from a cap returns the particle into the bulk, whereby the particle is moved in radial direction and placed at contact with

the disk. When unbinding from a sink, the particle transfers back to the cylindrical structure, i.e. becomes mobile again. Concerning implementation, particles bound to caps or sinks are treated as individual species, which enables the definition of different parameters and reactions for cylinder-bound and disk-bound species. This may be used, for example, to introduce cap-bound species representing particle clusters that "grow" by successively absorbing particles from the cylinder via a cascade of reactions, in order to model particle clustering at filament tips.

Since the problem of a diffusing 1D particle that interacts with a disk is mathematically equivalent to the problem of two interacting particles that move in 1D, here we may re-use the 1D Green's function with drift (2.64).

To model interactions with disks we introduce the following new domain types:

- *Cap Interaction* domain: a cylindrical domain that encloses an empty cap and a nearby cylinder-bound 1D particle. Next-event times are calculated from the 1D Green's function with drift and Rad-Abs boundary conditions.
- *Disk Surface Single* domain: a cylindrical domain that encloses a particle bound to a disk surface. The only possible next-events are unbinding reactions which are sampled from exponential distributions.
- *Mixed Pair 1D-Cap* domain: a cylindrical domain that encloses a cap with a bound particle and a nearby cylinder-bound 1D particle. Next-event times are calculated as for the *Cylindrical Surface Pair*, with drift and diffusion coefficient of the cap-bound partner set to zero.
- *Cylindrical Surface Sink* domain: a cylindrical domain that contains a sink and a proximate cylinder-bound particle. For this case we calculate the Green's function explicitly in section 2.5.

Sketches of these new domain types are shown in Figure 2.5.

Dynamical cylinders

While the aforementioned modifications allow for the inclusion of finite cylindrical structures into eGFRD, these are still assumed to be static. In reality, macromolecular filaments are dynamical structures which exhibit interchanging phases of growth and shrinkage. For microtubules, this mechanism is known as dynamic instability and has been extensively studied in both experiment [73, 74, 75, 76] and theory [77, 78, 79, 80].

We present a concept to include cylinders with length dynamics into eGFRD, with detailed description of required new domain and event types, in appendix section 2.C. The concept will be fully implemented in future work.

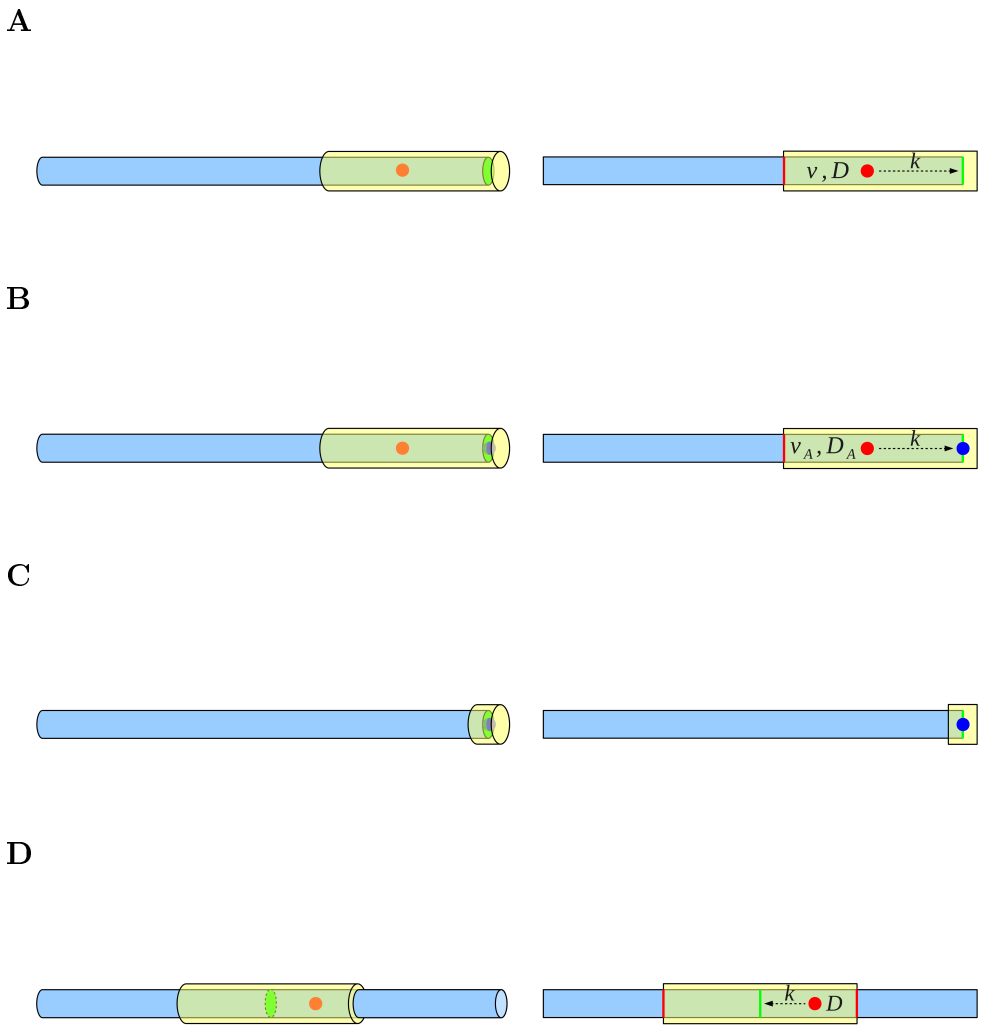

Figure 2.5: New protective domain types on finite 1D structures. The cylindrical surface is limited by a reactive cap at its right end (green colour). (A) *Cap Interaction* domain; (B) *Mixed Pair 1D-Cap* domain; (C) *Disk Surface Single* domain, here shown for a particle on a cap; (D) *Cylindrical Surface Sink* domain. Right panels show sections of 3D objects along the common cylinder axis. Absorbing boundaries are highlighted by red, radiative boundaries by green. Note that drift velocities (v, v_{A}, v_{B}) can be towards any cylinder end.

2.5 Green's function for 1D diffusion with a reactive sink

In transcription activation, transcription factors can perform a diffusive search for their binding site on the DNA [62, 63, 64]. To be able to model such and similar 1D random search processes in GFRD, we introduced sink structures that mark point-sites at which particles can react while diffusing over the cylindrical structure that they are bound to. In order to isolate this interaction from interactions with other particles on the cylinder we further introduced new domains (*Cylindrical Surface Sink* domains) that only contain a sink and the closeby particle. Exits from these domains then can happen via two different events: either the particle hits the (absorbing) boundaries of the domain, or it binds to the sink. For the case without particle drift, we present here the Green's function for this problem. One complication here is that the particle may diffuse over the sink without being absorbed. It is, however, possible to incorporate this feature into the mathematical derivation by imposing the correct probability flux balance at the sink position.

Assuming that the particle, starting from initial position $x = x_0$, can attach to the sink located at position x_s with an intrinsic rate k, the diffusive dynamics of the particle may be described via the modified diffusion equation:

$$\partial_\mathrm{t} p(x,t|x_0) = D\nabla^2 p(x,t|x_0) - k\delta(x-x_\mathrm{s})p(x,t|x_0) \tag{2.81}$$

with absorbing boundaries at $x = a$ and $x = b > x_\mathrm{s} > a$

$$p(a,t|x_0) = 0\ , \qquad p(b,t|x_0) = 0 \tag{2.82}$$

and initial condition

$$p(x,t=0|x_0) = \delta(x-x_0) \quad . \tag{2.83}$$

As with the 1D-Rad-Abs Green's function calculated in section 2.3.2, this problem may be solved separately for the subintervals of $[a,b]$ divided by the delta peaks, imposing continuity of $p(x,t|x_0)$ and discontinuity of its derivative at the junction points. Here it is convenient to consider the intervals left and right to the sink and to account for the initial condition directly by an adequate ansatz for the part that contains the starting point x_0. Continuity-discontinuity relations then only have to be imposed at x_s.

Let us denote the solution on interval $[a, x_\mathrm{s}]$ by $p_-(x,t|x_0)$ and the solution on $[x_\mathrm{s}, b]$ by $p_+(x,t|x_0)$. By integrating (2.81) over an ϵ-interval around the sink and taking the limit $\epsilon \to 0$ we obtain the discontinuity condition for the probability flux at $x = x_\mathrm{s}$:

$$\partial_\mathrm{x} p_-(x,t|x_0)\big|_{\mathrm{x=x_s}} - \partial_\mathrm{x} p_+(x,t|x_0)\big|_{\mathrm{x=x_s}} = -\frac{k}{D} p_-(x_\mathrm{s},t|x_0) \tag{2.84}$$

This equation simply states that the flux from/towards the left of the sink equals the flux from/towards the region right of it minus the reactive flux through the sink. Moreover, continuity requires:

$$p_-(x_\mathrm{s},t|x_0) = p_+(x_\mathrm{s},t|x_0) \tag{2.85}$$

Again this problem is most conveniently solved in LAPLACE space. The homogenous version of the LAPLACE-transformed PDE reads:

$$s\hat{p}(x,s|x_0) = D\nabla^2\hat{p}(x,s|x_0) \tag{2.86}$$

Let us without loss of generality assume $x_0 \in [x_s, b]$ and that the sink is located at $x = x_s = 0$, implying $a = -|a| < 0$. Then we can make the following ansatz in LAPLACE space ($q \equiv \sqrt{\frac{s}{D}}$):

$$\begin{aligned}
\hat{p}_-(x,s|x_0) &= A_- \sinh(qx) + B_- \cosh(qx), && x < 0 \\
\hat{p}_+(x,s|x_0) &= A_+ \sinh(qx) + B_+ \cosh(qx) + \underbrace{\frac{1}{2Dq} e^{-q|x-x_0|}}_{\hat{p}_{\mathrm{free}}(x,s|x_0)}, && x > 0
\end{aligned} \tag{2.87}$$

Function $\hat{p}_+(x,s|x_0)$ contains the (LAPLACE-transformed) free solution for a point particle starting from $x = x_0$ and thus fulfills the initial condition by construction.

The coefficients $A_\pm$ and $B_\pm$ are calculated by applying the boundary and continuity-discontinuity conditions. Subsequently, the solution can be transformed back into the time-domain via the residue formula. This procedure is precisely the same as in 2.3.2 and therefore omitted here. The final solution reads, with $L \equiv b - a = b + |a|$,

$$p_-(x,t|x_0) = -2D \sum_{n=1}^{\infty} e^{-D\zeta_n^2 t} \sin\left(\zeta_n(|a| + x)\right) \frac{\zeta_n \sin\left(\zeta_n(b - x_0)\right)}{\Xi_n} \tag{2.88}$$

$$\begin{aligned}
p_+(x,t|x_0) = -2D \sum_{n=1}^{\infty} e^{-D\zeta_n^2 t} \sin\left(\zeta_n(b - \hat{x})\right) \times \\
\frac{D\zeta_n \sin\left(\zeta_n(|a| + \check{x})\right) + k \sin(\zeta_n(|a|) \sin(\zeta_n \check{x})}{\Xi_n}
\end{aligned} \tag{2.89}$$

with $\hat{x} \equiv \max(x, x_0)$, $\check{x} \equiv \min(x, x_0)$ and a common denominator:

$$\begin{aligned}
\Xi_n = D\left[L\zeta_n \cos(\zeta_n L) + \sin(\zeta_n L)\right] \\
+ k\left[b\cos(\zeta_n b)\sin(\zeta_n|a|) + |a|\cos(\zeta_n|a|)\sin(\zeta_n b)\right]
\end{aligned} \tag{2.90}$$

The numbers ζ_n are all real and positive and the roots of the equation

$$D\zeta_n \sin\left(\zeta_n L\right) + k \sin\left(\zeta_n|a|\right) \sin\left(\zeta_n b\right) = 0 \tag{2.91}$$

which, with the help of trigonometric relations and setting $\Delta L \equiv b - |a|$, may be written in the more convenient form:

$$D\zeta_n \sin\left(\zeta_n L\right) = \frac{k}{2}\left[\cos\left(\zeta_n L\right) - \cos\left(\zeta_n \Delta L\right)\right] \tag{2.92}$$

The necessity of interchanging x and x_0 in (2.89) when the sign of $(x - x_0)$ changes arises from the presence of $|x - x_0|$ in the ansatz for $p_+(x,s|x_0)$.

The survival probability for the whole domain $[a, b]$ is given by

$$S(t) = \int_{\mathrm{a}}^{x_\mathrm{s}=0} p_-(x, t|x_0)dt + \int_{x_\mathrm{s}=0}^{b} p_+(x, t|x_0)dt \tag{2.93}$$

and easily obtained by simple integration.

The next-event time τ_ν for the associated *Cylindrical Surface Sink* domain is sampled from $1 - S(t)$, as usual. The next-event type, i.e. whether the particle exits the domain by being absorbed at the sink or at one of the boundaries, is determined by comparing the probability fluxes through these exit channels at τ_ν. These are most conveniently calculated via:

$$\begin{aligned} q_\mathrm{s} &= kp_-(x_\mathrm{s}, \tau_\nu|x_0) = kp_+(x_\mathrm{s}, \tau_\nu|x_0) \\ q_\mathrm{a} &= -D\partial_\mathrm{x} p_-(x, \tau_\nu|x_0)\big|_{\mathrm{x=a}} \\ q_\mathrm{b} &= -D\partial_\mathrm{x} p_+(x, \tau_\nu|x_0)\big|_{\mathrm{x=b}} \end{aligned} \tag{2.94}$$

2.6 Acknowledgements

The calculations for the 1D Green's function with sink presented in section 2.5 were carried out together with J. PAIJMANS as part of his master's project. The author also thanks him for performing additional tests of the other 1D Green's functions presented in this chapter and for fruitful discussions.

J. PAIJMANS further is credited with the elaboration of the two-step Brownian Dynamics scheme sketched in section 2.1.4.

The authors thanks A. HOFFMANN for critical reading of this chapter.

2.A Appendix: Detailed coordinate-separation transform

The SMOLUCHOWSKI equation for the probability density function $p = p(\mathbf{r}_\mathrm{A}, \mathbf{r}_\mathrm{B}, t|\mathbf{r}_\mathrm{A0}, \mathbf{r}_\mathrm{B0}, t_0)$ of two diffusing particles A and B that can interact via a force $\mathbf{F}$ depending on their distance and move with different diffusion constants D_A and D_B is given by [68, 39]

$$\partial_\mathrm{t} p = \left[D_\mathrm{A}\nabla_\mathrm{A}^2 + D_\mathrm{B}\nabla_\mathrm{B}^2 + D_\mathrm{A}\nabla_\mathrm{A}\cdot\varphi\mathbf{F}(\mathbf{r}) - D_\mathrm{B}\nabla_\mathrm{B}\cdot\varphi\mathbf{F}(\mathbf{r})\right] p \tag{S2.1}$$

where $\mathbf{r}$ denotes the interparticle vector:

$$\mathbf{r} = \mathbf{r}_\mathrm{B} - \mathbf{r}_\mathrm{A} \tag{S2.2}$$

We define the weighted center-of-mass vector $\mathbf{R}$ as follows:

$$\mathbf{R} = \gamma\mathbf{r}_\mathrm{A} + \delta\mathbf{r}_\mathrm{B} \tag{S2.3}$$

Equations (S2.2) and (S2.3) define new coordinates $\mathbf{r}(\mathbf{r}_\mathrm{A}, \mathbf{r}_\mathrm{B})$ and $\mathbf{R}(\mathbf{r}_\mathrm{A}, \mathbf{r}_\mathrm{B})$. Notice that this is not a coordinate transformation in the strict sense, as in general $\mathbf{r}$ and $\mathbf{R}$ will not be orthogonal.

Moreover, we define the operators:

$$\nabla_\mathrm{r} \equiv \frac{\partial}{\partial\mathbf{r}} = \begin{pmatrix}\partial_{\mathrm{r}_1}\\ \partial_{\mathrm{r}_2}\\ \partial_{\mathrm{r}_3}\end{pmatrix}, \qquad \nabla_\mathrm{R} \equiv \frac{\partial}{\partial\mathbf{R}} = \begin{pmatrix}\partial_{\mathrm{R}_1}\\ \partial_{\mathrm{R}_2}\\ \partial_{\mathrm{R}_3}\end{pmatrix}. \tag{S2.4}$$

If the differential operator on the right side of (S2.1) equation can be written as a sum of ∇_r^2, ∇_r, ∇_R^2 and ∇_R, we may separate (S2.1) into two independent PDEs for $\mathbf{r}$ and $\mathbf{R}$ by a product ansatz for p. In the following we will calculate different options for the choice of coefficients γ and δ with which the above objective is reached.

Rewriting ∇_A and ∇_B

First we rewrite ∇_A and ∇_B in terms of ∇_r and ∇_R. Let $r_{\mathrm{A,i}} = r_{\mathrm{A,i}}(\mathbf{r}, \mathbf{R})$ denote the i-th component of the vector $\mathbf{r}_\mathrm{A}$, and r_j, R_k components of $\mathbf{r}$ and $\mathbf{R}$ respectively. Then the derivative of p with respect to $r_{\mathrm{A,i}}$ is

$$\begin{aligned}\frac{\partial p}{\partial r_{\mathrm{A,i}}} &= \sum_\mathrm{j}\frac{\partial p}{\partial r_\mathrm{j}}\frac{\partial r_\mathrm{j}}{\partial r_{\mathrm{A,i}}} + \sum_\mathrm{k}\frac{\partial p}{\partial R_\mathrm{k}}\frac{\partial R_\mathrm{k}}{\partial r_{\mathrm{A,i}}}\\ &= \sum_\mathrm{j}(-1)\delta_\mathrm{ij}\frac{\partial p}{\partial r_\mathrm{j}} + \sum_\mathrm{k}\gamma\delta_\mathrm{ik}\frac{\partial p}{\partial R_\mathrm{k}}\\ &= \gamma\frac{\partial p}{\partial R_\mathrm{i}} - \frac{\partial p}{\partial r_\mathrm{i}} = \left(\gamma\frac{\partial}{\partial\mathbf{R}} - \frac{\partial}{\partial\mathbf{r}}\right)_\mathrm{i} p\end{aligned} \tag{S2.5}$$

because r_i and R_i only depend on the component $r_{\mathrm{A,i}}$ with the same index i. Since this holds for every i, we have:

$$\nabla_\mathrm{A} = \gamma\nabla_\mathrm{R} - \nabla_\mathrm{r} \tag{S2.6}$$

Analogously, one obtains:

$$\nabla_{\mathrm{B}} = \delta\nabla_{\mathrm{R}} + \nabla_{\mathrm{r}} \tag{S2.7}$$

From this it follows that:

$$\begin{aligned}\nabla_{\mathrm{A}}^2 &= \gamma^2\nabla_{\mathrm{R}}^2 + \nabla_{\mathrm{r}}^2 - 2\gamma\nabla_{\mathrm{r}}\nabla_{\mathrm{R}} \\ \nabla_{\mathrm{B}}^2 &= \delta^2\nabla_{\mathrm{R}}^2 + \nabla_{\mathrm{r}}^2 + 2\delta\nabla_{\mathrm{r}}\nabla_{\mathrm{R}}\end{aligned} \tag{S2.8}$$

Here we use $\nabla_{\mathrm{r}}\nabla_{\mathrm{R}} = \nabla_{\mathrm{R}}\nabla_{\mathrm{r}}$, assuming the 2nd derivative of p with respect to any of its variables to be a continuous function in $\mathbb{R}^3$. The partial derivatives then may be interchanged by the theorem of CLAIRAUT & SCHWARZ.

Now that we have expressed ∇_{A} and ∇_{B} in terms of ∇_{r} and ∇_{R}, we can also rewrite the right side of the SMOLUCHOWSKI equation. First, for the case $\varphi = 0$, we get:

$$\begin{aligned}D_{\mathrm{A}}\nabla_{\mathrm{A}}^2 + D_{\mathrm{B}}\nabla_{\mathrm{B}}^2 = &\left(D_{\mathrm{A}} + D_{\mathrm{B}}\right)\nabla_{\mathrm{r}}^2 \\ &+ \left(\gamma^2 D_{\mathrm{A}} + \delta^2 D_{\mathrm{B}}\right)\nabla_{\mathrm{R}}^2 \\ &+ 2\left(\delta D_{\mathrm{B}} - \gamma D_{\mathrm{A}}\right)\nabla_{\mathrm{r}}\nabla_{\mathrm{R}}\end{aligned} \tag{S2.9}$$

Rewriting the force term separately yields:

$$\left(D_{\mathrm{A}}\nabla_{\mathrm{A}} - D_{\mathrm{B}}\nabla_{\mathrm{B}}\right)\cdot\varphi\mathbf{F} = \left[\left(\gamma D_{\mathrm{A}} - \delta D_{\mathrm{B}}\right)\nabla_{\mathrm{R}} - \left(D_{\mathrm{A}} + D_{\mathrm{B}}\right)\nabla_{\mathrm{r}}\right]\cdot\varphi\mathbf{F} \tag{S2.10}$$

To get rid of the mixed term containing $\nabla_{\mathrm{r}}\nabla_{\mathrm{R}}$ we can make any choice for γ and δ that fulfills

$$\delta = \frac{D_{\mathrm{A}}}{D_{\mathrm{B}}}\gamma \quad . \tag{S2.11}$$

Note that with this choice the force contribution (S2.10) only depends on the derivative with respect to the interparticle vector (∇_{r}).

Coefficient choice as in original GFRD

One possible choice for γ and δ, which is the the same as in the original version of GFRD, is the following:

$$\gamma \equiv \sqrt{\frac{D_{\mathrm{B}}}{D_{\mathrm{A}}}}, \qquad \delta \equiv \sqrt{\frac{D_{\mathrm{A}}}{D_{\mathrm{B}}}} \tag{S2.12}$$

This yields

$$\mathbf{R} = \sqrt{\frac{D_{\mathrm{B}}}{D_{\mathrm{A}}}}\cdot\mathbf{r}_{\mathrm{A}} + \sqrt{\frac{D_{\mathrm{A}}}{D_{\mathrm{B}}}}\cdot\mathbf{r}_{\mathrm{B}} \tag{S2.13}$$

and

$$D_{\mathrm{A}}\nabla_{\mathrm{A}}^2 + D_{\mathrm{B}}\nabla_{\mathrm{B}}^2 = \left(D_{\mathrm{A}} + D_{\mathrm{B}}\right)\left(\nabla_{\mathrm{r}}^2 + \nabla_{\mathrm{R}}^2\right) \quad . \tag{S2.14}$$

The same prefactor also appears in the force term

$$(D_\mathrm{A}\nabla_\mathrm{A} - D_\mathrm{B}\nabla_\mathrm{B}) \cdot \varphi\mathbf{F} = -\left(D_\mathrm{A} + D_\mathrm{B}\right)\nabla_\mathrm{r} \cdot \varphi\mathbf{F} \tag{S2.15}$$

so that equation (S2.1) simplifies as follows:

$$\partial_\mathrm{t} p = \left(D_\mathrm{A} + D_\mathrm{B}\right)\left(\nabla_\mathrm{r}^2 + \nabla_\mathrm{R}^2 - \nabla_\mathrm{r} \cdot \varphi\mathbf{F}\right) p \tag{S2.16}$$

Here we can separate the equation by the product ansatz $p(\mathbf{r}, \mathbf{R}, t|\mathbf{r}_0, \mathbf{R}_0, t_0) = p_\mathrm{r}(\mathbf{r}, t|\mathbf{r}_0, t_0)p_\mathrm{R}(\mathbf{R}, t|\mathbf{R}_0, t_0)$ into two equations describing two independent diffusion processes (here with the same diffusion constant $D_\mathrm{A} + D_\mathrm{B}$):

$$\partial_\mathrm{t} p_\mathrm{r} = \underbrace{\left(D_\mathrm{A} + D_\mathrm{B}\right)}_{D_\mathrm{r}}\left(\nabla_\mathrm{r}^2 - \nabla_\mathrm{r} \cdot \varphi\mathbf{F}\right) p_\mathrm{r} \tag{S2.17}$$

$$\partial_\mathrm{t} p_\mathrm{R} = \underbrace{\left(D_\mathrm{A} + D_\mathrm{B}\right)}_{D_\mathrm{R}}\nabla_\mathrm{R}^2\, p_\mathrm{R} \tag{S2.18}$$

Note that, as expected, the force contribution is present only in the equation for the interparticle vector $\mathbf{r}$.

Coefficient choice as in eGFRD

The following slightly different choice for γ and δ

$$\gamma \equiv \frac{D_\mathrm{B}}{D_\mathrm{A} + D_\mathrm{B}}, \qquad \delta \equiv \frac{D_\mathrm{A}}{D_\mathrm{A} + D_\mathrm{B}} \tag{S2.19}$$

leads to:

$$\begin{aligned} D_\mathrm{A}\nabla_\mathrm{A}^2 + D_\mathrm{B}\nabla_\mathrm{B}^2 &= \left[\frac{D_\mathrm{A}D_\mathrm{B}^2 + D_\mathrm{B}D_\mathrm{A}^2}{\left(D_\mathrm{A} + D_\mathrm{B}\right)^2}\right]\nabla_\mathrm{R}^2 + \left(D_\mathrm{A} + D_\mathrm{B}\right)\nabla_\mathrm{r}^2 \\ &= \left(\frac{D_\mathrm{A}D_\mathrm{B}}{D_\mathrm{A} + D_\mathrm{B}}\right)\nabla_\mathrm{R}^2 + \left(D_\mathrm{A} + D_\mathrm{B}\right)\nabla_\mathrm{r}^2 \end{aligned} \tag{S2.20}$$

Everything that has been said for the previous choice of γ and δ also applies to this case, except for the fact that $\mathbf{R}(\mathbf{r}_\mathrm{A}, \mathbf{r}_\mathrm{B})$ now has a different weighting as before:

$$\mathbf{R} = \frac{D_\mathrm{B}\mathbf{r}_\mathrm{A} + D_\mathrm{A}\mathbf{r}_\mathrm{B}}{D_\mathrm{A} + D_\mathrm{B}} \tag{S2.21}$$

Therefore, also the diffusion constant D_R now is different from D_r. Using the same separation ansatz as before we arrive at:

$$\begin{aligned} \partial_\mathrm{t} p_\mathrm{r} &= \left(D_\mathrm{A} + D_\mathrm{B}\right)\left(\nabla_\mathrm{r}^2 - \nabla_\mathrm{r} \cdot \varphi\mathbf{F}\right) p_\mathrm{r} \\ \partial_\mathrm{t} p_\mathrm{R} &= \left(\frac{D_\mathrm{A}D_\mathrm{B}}{D_\mathrm{A} + D_\mathrm{B}}\right)\nabla_\mathrm{R}^2\, p_\mathrm{R} \end{aligned} \tag{S2.22}$$

Prescribing an arbitrary centre-of-mass diffusion constant

For completeness we briefly describe how to choose γ and δ in order to ensure that D_R is equal to an arbitrary prescribed diffusion constant D_C, if desired. D_C might be, for example, the diffusion constant of the product of the $A + B \to C$ reaction.

In this case γ and δ have to obey the two equations:

$$D_\mathrm{R} = \gamma^2 D_\mathrm{A} + \delta^2 D_\mathrm{B}, \qquad \delta = \frac{D_\mathrm{A}}{D_\mathrm{B}}\gamma \tag{S2.23}$$

Combining these we obtain:

$$D_\mathrm{R} = \gamma^2 D_\mathrm{A}\left[1 + \frac{D_\mathrm{A}}{D_\mathrm{B}}\right] \stackrel{!}{=} D_\mathrm{C} \tag{S2.24}$$

Since all involved quantities are positive real numbers, it follows that:

$$\gamma = \sqrt[+]{\frac{D_\mathrm{C}}{D_\mathrm{A}\left(1 + \frac{D_\mathrm{A}}{D_\mathrm{B}}\right)}} \qquad \Rightarrow \qquad \delta = \frac{D_\mathrm{A}}{D_\mathrm{B}}\gamma = \sqrt[+]{\frac{D_\mathrm{C}}{D_\mathrm{B}\left(1 + \frac{D_\mathrm{B}}{D_\mathrm{A}}\right)}} \tag{S2.25}$$

This combination of γ and δ indeed leads to:

$$\begin{aligned} D_\mathrm{R} = D_\mathrm{A}\gamma^2 + D_\mathrm{B}\delta^2 &= \frac{D_\mathrm{C}}{1 + \frac{D_\mathrm{A}}{D_\mathrm{B}}} + \frac{D_\mathrm{C}}{1 + \frac{D_\mathrm{B}}{D_\mathrm{A}}} \\ &= \frac{D_\mathrm{B}D_\mathrm{C} + D_\mathrm{A}D_\mathrm{C}}{D_\mathrm{A} + D_\mathrm{B}} = D_\mathrm{C} \end{aligned} \tag{S2.26}$$

Since γ and δ are always real and positive, except for the (usually uninteresting) cases $D_\mathrm{A} = 0$ or $D_\mathrm{B} = 0$, one can indeed always find a coordinate transform for which D_R matches an arbitrary diffusion coefficient, while $D_\mathrm{r} = D_\mathrm{A} + D_\mathrm{B}$.

2.B Appendix: Domains in eGFRD

2.B.1 Domain classtree

Figure S2.1 shows the complete class tree of the domain classes employed by the new version of eGFRD that features transport and reactions in 1D and 2D, including the new domain types introduced in chapters 2 and 3.

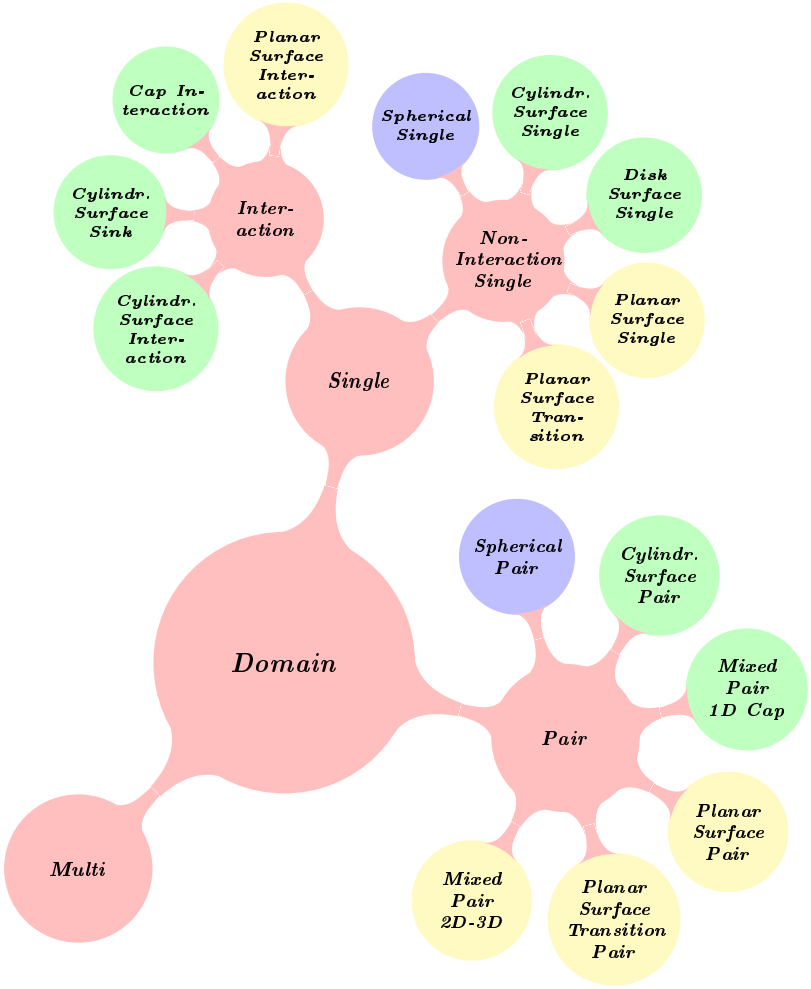

Figure S2.1: Domain class tree. Blue circles are domain types used to simulate reactions and diffusion purely in 3D. Domain types employed for interactions with and reaction-diffusion on 1D rods are in green, whereas yellow marks domain types used for 2D interactions and reaction-diffusion. Red color marks abstract superclasses.

2.B.2 Domain making in eGFRD

Principal domain making strategy

The governing principle in constructing and sizing of domains in eGFRD is to minimize the computational cost associated with this process. Domain making consists of the following successive steps:

1. Determine which type of domain to construct.
2. Determine the available space for the domain (i.e. its shell).
3. Construct the domain with an optimally sized shell.
4. Draw the next-event time and type for the newly constructed domain.
5. Re-schedule the domain in the central scheduler.

While the cost of the first and last step is roughly the same for all domains, it may vary among different domain types for the other steps. In general, cylindrical domains are more expensive to construct than spherical domains because of the increased computational effort for scaling up cylinders within a constellation of other cylinders and spheres. Similarly, *Pair* domains are more expensive than *Single* domains because they require an additional coordinate transform and employ Green's functions which are mathematically more complex.

It is unfeasible to foresee all possible constellations that may occur during eGFRD simulations as required for a real quantitative optimization of the domain making rules. The strategy in defining a unique set of functional rules therefore is to minimize the likelihood of situations that lead to the waste of computational cost, such as repeated reconstruction of domains and construction of expensive domains when it is not strictly advantageous.

Social upsizing prevents premature and mutual bursting

Particular care must be put into determining the optimal size of the domain. In principle we want to construct domains as big as possible because their next-event time directly correlates with their size. However, when we size up a large domain such that it will protrude into the direct vicinity of a very small domain, the latter will most likely be updated long before the next event time of the freshly constructed large domain. This may induce premature bursting of the large domain which then has to be reconstructed from an almost identical situation as before after insignificant time progress, wasting the initial investment of domain making cost. Therefore domains should not be sized up to the maximal available space in any given situation but in a "social" manner, i.e. leave some space for their neighbour domains to avoid very small domains in their own direct vicinity.

In particular it is important to prevent repeated mutual bursting of two newly constructed adjacent *Single* domains, which may even result in an infinite cycle of domain (re)construction and bursting. Repeated mutual bursting can occur when two particles are at a small distance, yet sufficiently far away to enable the construction

of two *Single* domains, and the formation of a *Pair* is disallowed for other reasons (e.g. presence of obstacles). Since domains are sized up in a successive order, using the maximally available space for the first *Single* domain (A) would result in a very small size of the second (B), causing immediate update of B with negligible particle displacement. This in turn would force bursting of domain A in order to size up the B domain again, which would restart the whole process all over from B. This example demonstrates that maximizing domain size is not the same as optimizing it.

A minimal Single domain size controls switching to Brownian Dynamics

In section 2.1.4 we explain why it is necessary to switch from eGFRD to Brownian Dynamics when propagating particles under crowded conditions. Yet, it is not a priori clear when this switch should be performed. In principle it should be done when the computational cost for *Single* construction divided by the maximal displacement within the domain, which is correlated to domain size, becomes larger than the cost to sample a trajectory covering the same distance with Brownian Dynamics. Since in GFRD *Single* construction cost is variable, it is hard to devise a general rule. Notwithstanding, it is clear that a minimal *Single* has to be defined for proper working of the algorithm. We decided to make this a simulation parameter, the details of which will be described in more detail in the following text.

Summarized domain making objectives

The abovementioned compiles into the following set of simple objectives for efficient domain making rules:

- Construct *Pair* and *Interaction* domains only when interaction is likely, i.e. when particles are close to other particles or reactive surfaces.
- Construct domains socially, i.e. reserve some space for neighbouring domains in order to prevent premature or mutual bursting.
- Construct *Multi* domains (i.e. fall back into Brownian dynamics) if construction of a minimal-size *Single* is impossible.

In order to transform these rules into an applicable algorithm we introduced two length factors which will determine when to start constructing *Pairs* or *Interactions* and when to go into the Brownian dynamics mode during runtime.

Two length factors balance the domain making behaviour

Let us define the following two dimensionless constants:

- $\beta \equiv$ "single-shell factor"
- $\mu \equiv$ "multi-shell factor"

For a given particle radius R these two factors define the half-size βR of the minimal *Single* shell and the radius μR of the (always spherical) *Multi* shell of that

particle, respectively. Note that the minimal *Single* shell can be either a sphere or a cylinder, depending on whether the particle is a 3D, 2D or 1D species. The requirements $\beta \geq 1$ and $\mu \geq 1$ are obvious. Since a *Multi* shell shall never be constructed when there is enough space for a minimal *Single* shell, we also require $\beta > \mu$.

Let R_0 be the radius of a particle P_0 for which we want to construct a domain, R_1 the radius of its nearest neighbour particle P_1 and $\sigma \equiv R_0 + R_1$. Then, based on β and μ, we define the following lengths for P_0:

- the "reaction horizon" $\equiv \beta R_0$
- the "multi horizon" $\equiv \mu R_0$

and, as specializations of the above:

- the "pair horizon" $\equiv \beta\sigma$
- the "surface horizon" $\equiv$ "reaction horizon" $= \beta R_0$
- the "burst horizon" $\equiv$ "burst radius" $\equiv$ "reaction horizon" $= \beta R_0$
- the "multi-partner horizon" $\equiv \mu\sigma$

Different naming highlights different purpose for these of the above quantities that are equal to each other.

The reaction horizon is used to determine when a *Pair* or *Interaction* domain should be constructed instead of a *Single* domain. The multi horizon defines when *Single* construction should be dropped in favor of *Multi* construction. The pair horizon and surface horizon are specifications of the reaction horizon for *Pair* and *Interaction Single* formation: while an *Interaction* is formed when a surface is within the reaction horizon, a *Pair* construction is attempted only when the reaction horizons of the two involved particles overlap, i.e. when the center of mass of P_1 is within the pair horizon of P_0. Similarly, the algorithm will switch into Brownian Dynamics mode when a surface is within the multi horizon of P_0 or when the multi horizons of P_0 and P_1 overlap, i.e. when P_1 is within the multi-partner horizon of P_0.

The burst horizon defines the volume within which a particle will burst neighbouring domains. Since the objective of bursting is to generate space for at least a minimal *Single* shell the burst horizon should be at least as big as the reaction horizon. Since there is no evident necessity to make it bigger than the reaction horizon, we conveniently set these lengths to be equal.

Practically β and μ can be used to tune the overall behaviour and performance of domain making: Increasing μ will prompt the simulation to switch to Brownian Dynamics earlier. Whether this is advantageous or not depends the crossover radius at which construction of small *Single* domains yields a smaller average simulation time advance per computational cost unit than the construction of *Multi* domains. In a similar way, whether a larger or smaller β is favorable depends on the average likelihood of reactions in the system. Since the latter depend on the parameters, there is no obviously optimal choice for β and μ. We find that $\beta \in [2, 3]$ and $\mu \in [\sqrt{3}, 2]$ gives reasonable performance.

Domain making algorithm

We can now compile the abovementioned postulations and definitions into a well-defined algorithm for domain making. Let us imagine a particle which just exited from whatever domain type after an update. An update can be either triggered by a next-event picked from the scheduler (i.e. a reaction, domain exit or surface interaction) or by premature bursting of neighbouring particles induced in the aftermath of such scheduler event. The particle by default is put into the system as a *Non-Interaction Single* with a shell that just envelopes the particle. Note that this "zero-shell" is spherical for 3D particles and cylindrical for 2D and 1D particles. We will call a *Single* with a zero-shell a "*Zero-Single*". Each *Zero-Single* is put into the scheduler with zero next-event time ($dt = 0$) in order to reconstruct its domain immediately after it was produced.

We then perform the following order of actions to construct a new domain:

1. **Bursting**: Burst any neighbouring "intruder", i.e. a domain that intrudes into the burst radius of the particle, with the exception of *Multi* domains and other *Zero-Singles*, i.e. domains which are yet to pass through the domain making procedure themselves. By default the burst radius is equal to the reaction horizon. Burst recursively, i.e. whenever a bursted intruder has intruders within its own reaction horizon, also burst these. The following steps then are repeated for each *Zero-Single* present in the system after bursting.

2. **Reaction/interaction attempt**: Compile a list of all potential interaction partners (particles or reactive surfaces). Pick the closest interaction partner and try a reaction (with particles) or interaction (with surfaces) if the closest partner is within the specified reaction or interaction horizon. If a minimal reaction (*Pair*) domain or *Interaction* domain can be constructed, size it up socially to the maximal available space and go directly to step (4.).

3. ***Single* domain upsizing attempt**: If a *Pair* or *Interaction* could not be constructed, yet the closest partner is within the multi horizon of the *Non-Interaction Single*, then (recursively) construct a *Multi* domain (as specified further below) and proceed directly to step (4.). Else, size up the *Non-Interaction Single* domain socially to the maximally available space and continue.

4. **Re-scheduling**: For the constructed domain type determine the next-event time and type and reinsert this information into the scheduler.

5. **Repeat** the whole procedure for the next *Zero-Single* until there are no more *Zero-Singles* in the scheduler.

The pseudo-code of the domain making algorithm is shown in Algorithm S1.

Algorithm S1 The eGFRD domain making algorithm.

$Z \leftarrow$ *Zero-Single*
while $z \in Z$ **do**

  for all domain in burst radius of z **do**
    if domain is **not** *Multi* **and** $\mathrm{dt}(\mathrm{domain}) > 0$ **then**
      $Z_{\mathrm{bursted}} \leftarrow$ burst domain recursively
      $Z \cup Z_{\mathrm{bursted}}$
    end if
  end for

  $S \leftarrow$ {neighbouring surfaces of z}
  $P \leftarrow$ {neighbouring particles of z}
  $c \leftarrow$ closest object $n \in S \cup P$

  if $c \in S$ **and** c in surface horizon of z **then**
    successful $\leftarrow$ try interaction of z with c
  else if not successful **and** $c \in P$ **and** c in pair horizon of z **then**
    successful $\leftarrow$ try to form *Pair* (z, c)
  else if not successful **and** c out of multi horizon of z **then**
    successful $\leftarrow$ try to scale up shell of z
  else if not successful **then**
    form *Multi* from z with c recursively
  end if

  re-schedule z
  remove z from Z

end while

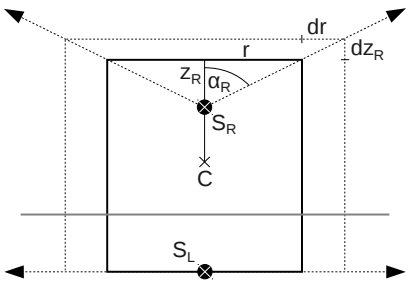

Figure S2.2: Cylinder scaling in eGFRD. The cylinder is scaled differently on its two sides (L and R) from two separate scale centers S_{L} and S_{R} which here do not coincide with the center point (C). For each side, the scale angle (α_{L}, α_{R}) defines the aspect ratio at scaling, i.e. how the respective height (z_{L}, z_{R}) scales with the cylinder radius (r). In the given example, $\alpha_{\mathrm{L}} = \pi/2$, meaning that z_{L} ($= 0$) remains constant upon changing r.

Multi construction

In eGFRD *Multis* are contingent three-dimensional objects made up from either one spherical *Multi* shell or a set of overlapping spherical *Multi* shells. The radius of a *Multi* shell is equal to the particle radius plus the reaction length multiplied by the multi-shell factor $\mu > 1$. *Multi* domains are constructed recursively: When a *Zero-Single* z has been determined to form a *Multi* object it checks for objects within its surroundings. Any other *Zero-Single* z' that is within the common multi horizon $\mu(R_z + R_{z'})$ will be added to the *Multi*. Then, for each z' that was added, the same check is performed for its surroundings, ignoring z. This is repeated until no further *Zero-Singles* can be added to the *Multi* object. Note that *Multi* shells in such constellations in principle can overlap with more than one other *Multi* shells. If there are only surfaces within the horizon the *Multi* will consist of only one *Multi* shell, the one around z.

The test-shell concept

In order to prevent double effort, in eGFRD the sizing of a domain shell upon domain (re)construction is decoupled from sampling of next-event information from the Green's function. This is achieved by using "test shells". In a particular situation in which a new domain has to be created, the simulator first attempts to determine the maximal size of the tentative test shell of the domain, taking into account the required shell geometry (cylinderical or spherical) and particular scaling parameters (e.g. the scale aspect ratio of cylinders). Starting from a (predefined) maximal shell size, the test shell then is scaled down successively with respect to each neighboring shell via collision detection. During the collision detection step the maximal dimensions of the test shell that does not lead to an overlap with the particular other domain shell are calculated (see subsequent section for more detail). If at the end of the scaling procedure the dimensions of the test shell are not smaller than the required minimal dimensions (determined by the factors β and μ defined further above and particle radii) a new domain object is parametrized with the test shell, and only after this step its next-event information is sampled. In the opposite case the construction of the respective domain type is rejected and the algorithm proceeds by attempting the construction of another domain type (e.g. *Single* or *Multi*).

Shell collision detection

Considerable computational effort has to be put into detection of collisions between a scaled test shell and another (static) shell. While this problem is trivial when scaling spheres or cylinders against spheres or parallel cylinders against each other, it is, maybe surprisingly, less straightforward for arbitrarily oriented and even orthogonal cylinders. Note that in eGFRD cylinder scaling is performed subject to a fixed (but in principle arbitrary) "scale aspect ratio" (defining a certain "scale angle"), which links the change in cylinder height to the change in the radius. The aspect ratio is usually set by the requirement of equalizing expected first passage times of the enclosed particle towards the cap and the tube of the cylindrical shell; as illustrated

by Figure S2.2, the scale angle may differ for the two opposite sides of the cylinder[1]. In general, also the reference points of the scaling ("scale centers") do not coincide with the midpoint of the cylinder, particularly in cases in which scale angles are indeed different on both sides. Thus, scaling a cylindrical shell in eGFRD conceptually consists of scaling the two sides of the cylinder separately, albeit linked via the common radius.

To scale orthogonal cylinders against each other in eGFRD we consider the two-cylinder problem in a standardized cartesian coordinate system centered at the midpoint of the scaled cylinder, with x-base-vector pointing towards the midpoint of the static cylinder and z-base-vector coinciding with the axis of the scaled cylinder. We then determine the specific type of collision that may occur upon scaling up the cylindrical test shell. There are seven possible collision types:

1. TF: the tube of the scaled cylinder hits the flat side of the static cylinder.
2. TT: the tube of the scaled cylinder hits the tube of the static cylinder.
3. TE: the tube of the scaled cylinder hits the edge[2] of the static cylinder.
4. FT: the flat side of the scaled cylinder hits the tube of the static cylinder.
5. ET: the edge of the scaled cylinder hits the tube of the static cylinder.
6. EE: the edge of the scaled cylinder hits the edge of the static cylinder.
7. None: no collision possible in the given scenario[3].

Identification of the collision type is facilitated by comparing the location of the projected midpoint of the scaled cylinder to the projected edges of the static cylinder in the xy-plane of the standardized coordinate system (in which the scaled cylinder appears circular and the static cylinder rectangular). Certain respective locations exclude certain collision types; for example, if the midpoint of the scaled cylinder is within the rectangular projection of the static cylinder, the collision must be of type FT (given that the height is scaled). Once the collision type is known, the maximal dimensions of the scaled cylinder are determined taking into account its "intrinsic" scaling properties (scale angle, location of scale center, minimal size). This is mostly achieved via straightforward geometric calculations. For collision type EE a closed form for the new dimensions could not be obtained; the values are therefore calculated from an implicit equation using a numerical rootfinder. The detailed calculations are part of the eGFRD technical documentation and beyond the scope of this thesis.

A concise scheme for scaling arbitrarily oriented eGFRD-type cylinders against each other is yet to be devised.

[1] This is e.g. the case for the shell of the *Planar Surface Interaction* domain (see section 3.2.1), the height of which is scaled only on the side of the planar surface facing the particle, while the height on the opposite side is kept fixed when the radius is scaled. This is the example shown in Fig. S2.2, where the gray line represents a planar surface.

[2] defined as the circular line that separates cylinder tube and flat side

[3] This e.g. may occur in cases in which only the radius or height are scaled.

2.B.3 Convergence issues affecting domain construction

The Green's functions, survival probabilities, cumulative PDFs and the expressions for the boundary fluxes used in eGFRD typically have the common form

$$C \cdot \sum_{\mathrm{n}=0}^{\infty} e^{-\zeta_{\mathrm{n}}^2 Dt} X_{\mathrm{n}} \tag{S2.27}$$

where C is constant and X_{n} does not depend on t. It can be shown that ζ_{n}^2, to a good approximation, scales linearly with n and inversely with the domain size L, while typically $|X_{\mathrm{n}}| \sim 1$. Convergence of these sums thus is dominated by the exponential terms. We found that it is severly hampered for evaluation times t which are small on the typical timescale of the domain, i.e. the mean time required to traverse it by diffusion with diffusion constant D. This is the case when the distance Δ of the particle to the closest boundary becomes very small. Then evaluation times are of the order of $t_\Delta = \Delta^2/2dD$, where d is the dimensionality. A fair estimate for the number n of summation terms needed to reach a desired convergence threshold ε follows from:

$$e^{-\left(\frac{cn}{L}\right)^2 Dt} < \varepsilon \qquad \Leftrightarrow \qquad n > \frac{L\sqrt{1/\varepsilon}}{c\sqrt{Dt}} \tag{S2.28}$$

where we approximate $\zeta_{\mathrm{n}} = cn/L$ with $c = const.$ Inserting t_Δ into the above equation yields

$$n_\Delta > \frac{L}{\Delta} \cdot const \tag{S2.29}$$

showing that the required number of terms to reach a predefined convergence accuracy scales inversely with the distance Δ to the closest boundary. Therefore it should be avoided to construct domains in a way that Δ/L is small; optimally domains should be constructed in a way that distances between the starting point of the diffusing particle and the domain boundaries are approximately equal.

In practice this is handled in two ways: Whenever particles start very close to radiating or absorbing boundaries we construct a domain that does not use all available space but is only sized up to $L \simeq 2\Delta$. While this requires the succesive creation of undersized domains (resulting in minor next-event times) in order to elongate the distance between the reactive boundary and the particle, it overcomes the above-mentioned convergence issues by keeping Δ/L constant. Alternatively, we scale domains up as much as possible and, where available, employ Green's functions that are bounded unilaterally, i.e. neglect the distant second boundary. These Green's functions typically are finite sums, which facilitates their implementation and computation, and in the above case approximate the double-bounded solutions very well.

2.C Appendix: Dynamical cylinders

2.C.1 Abstracting dynamical properties of microtubules

A further step towards a more accurate representation of microtubules in eGFRD is to allow for dynamical cylindrical surfaces which–in a coarse-grained fashion–reflect the dynamics of microtubules. Here we present a concept to incorporate dynamical cylinders into eGFRD.

Microtubule dynamics are characterized by permanent length changes via a process called dynamic instability [73, 74, 75, 76]: The microtubule tip alternates between phases of growth and shrinkage; the latter are induced by sporadic "microtubule catastrophies" that lead to an almost instantaneous shortening of the microtubule by a large fraction of its length, occasionally even to its complete disappearance. Catastrophies are–to a good approximation–Poissonian events that happen with a certain frequency which may depend on other factors, such as forces exerted onto the microtubule [81] and the presence of tip-tracking proteins [82, 83, 44].

The arguably most simple way to implement dynamic instability into eGFRD is to allow for length fluctuations of cylindrical surfaces that grow at a constant speed v_g and retract instantaneously to zero length at a constant catastrophy rate k_c. Next-event times for catastrophy events then can be sampled from an exponential distribution, while growth is linear and future length therefore easy to predict. However, since the cylinders typically carry particles enclosed by domains with well-defined next-event times, which moreover may interact with the growing tip, more care is required to integrate growth and shrinkage events with events produced by particle domains. In the following sections we first describe how catastrophies of dynamical cylinders can be treated within the current eGFRD framework. We then introduce growth events, produced by several new "growth" domain types that take into account particles bound to or interacting with a growing cylinder cap, as described in more detail further below. Finally, we give a brief summary of the dynamical cylinder concept elaborated here.

2.C.2 Including growth and catastrophies into eGFRD

We assume that the succession of microtubule catastrophies is a Poisson process with constant catastrophy rate k_c. Next-event times for catastrophies then are easily sampled via $\tau_c = -k_c \ln(\mathcal{R})$, where $\mathcal{R}$ is a random number from the uniform distribution on $[0, 1]$. For each cylindrical surface, τ_c is the lifetime of the cylinder and as such an upper cut-off for growth next-event times.

In the event of a catastrophy (*"Cylindrical Surface Catastrophy"*) the length of the cylindrical surface is immediately set to zero and all domains associated with that surface are bursted, i.e. their position is propagated up to the time of catastrophy τ_c before they are converted to cytoplasmic zero-singles.

Cylinders grow at constant speed within cylindrical growth domains

In order to shield the growing cylinder tip from interference by particles that are in the way we construct cylindrical growth domains in the extension of the cylinder surface

beyond its growing end ("growth volume"), with a certain length L_g determined by the specific constellation in the neighborhood of the growth domain. Here we first consider the most simple growth domain, the *"Cylindrical Surface Cap Growth"* domain, which encloses only the growing tip and the growth volume; further growth domains that also contain cylinder-bound particles are the subject of the forthcoming sections. We define the *"Cylindrical Surface Growth"* event to occur when the growing cap of the cylindrical surface reaches the distant end of the growth domain. For constant growth velocity v_g we can easily calculate the length $L(t|t < \tau_c)$ of the cylinder at any future time t given that a catastrophy did not happen until that time. The next-event time of the growth event then simply is given by $\tau_g \equiv L_g/v_g$. To avoid that the growth domain becomes an artificial obstacle for diffusing particles we allow the growth domain to be bursted by nearby particles when the growth domain is within the burst radius of the particles. This results in a length change $\Delta L < L_g$ and creates a situation in which the particles close to the growing cylindrical surface correctly detect the free space available to them.

Whenever obstacles such as surfaces or particle domains are in the way of the growing cylinder, the growth domain is constructed up to the closest interfering object in the direction of cylinder growth (i.e. along the extended cylinder axis). When a growth domain with minimal size cannot be constructed any more, both the length changes of the cylinder and–if the obstacles are particle domains–the displacements and reactions of intruding particles are simulated via Brownian dynamics. Once the intruders have moved out of the growth volume of the cylindrical surface, construction of a new growth domain may be attempted. To avoid instantaneous re-bursting of a newly constructed growth domain, it is wise to propagate the particles in BD mode until their distance is larger than their burst radius (reaction horizon).

Binding to a growing cylinder cap

In section 2.4 we have described how the 1D Green's function with drift derived in section 2.3 is used to sample next-event times and positions for a particle that diffuses (with diffusion constant D) and drifts (with velocity v) on a finite, static cylindrical surface and binds to the cylinder cap with an intrinsic reaction rate. This principle can be straightforwardly extended to the case of dynamical cylinders. For constant cylinder growth velocity v_g, the problem can be easily transformed into the reference frame of the moving cap by substituting the drift velocity v in the Green's function with $v - v_g$. Note that this then also assumes that the absorbing boundary of the cap binding domain is not static any more, but trails behind the particle at a velocity v_g. This has to be taken into account when sampling a new particle position x on the cylinder axis at a time τ: position x has to be post-processed by adding $\Delta x = v_g\tau$, the length increase of the growing cylinder until time τ. Note that τ may be a time at which the domain is bursted, and thus arbitrary.

To isolate the problem from exterior influence, we can encapsulate the particle and the growing cap by a (cylindrical) *"Cylindrical Surface Growing Cap Interaction"* domain that extends beyond the cap as far as possible, i.e. using up all available space in the direction of the growing cylindrical surface. As described for the *Cylindrical Surface Cap Growth* domain (see previous subsection), the length of this extension

defines the next-event time τ_g for the *Cylindrical Surface Growth* event. The next-event time τ_ν for the *Cylindrical Surface Growing Cap Interaction* domain then is given by the minimum of τ_{dd}, the next-event time sampled from the diffusion-drift Green's function with the modified drift, τ_g and τ_s, which is the tentative time of the next monomolecular reaction of the particle.

Similarly, we can define a *"Cylindrical Surface Growing Cap Single"* domain for a particle that is bound to the cap of a growing cylinder. Again we construct a cylindrical domain that encloses the particle and as much of the space in the direction of the growing cylinder as possible. Here the next-event time τ_ν is the minimum of τ_g (cylinder growth) and τ_s (monomolecular reaction). For any τ_ν, both the cap and the particle are displaced by $\Delta x = v_g \tau_\nu$; when $\tau_\nu = \tau_s$, the particle in addition is displaced orthogonally and placed at contact with the cap at a random angle.

To end with, the case of a cylinder-bound particle interacting with a particle on the growing cylinder cap can be treated in analogy to the *Cylindrical Surface Growing Cap Interaction* defined above. As before, we can create a cylindrical domain (*"Mixed Pair 1D-Growing Cap"*) that encloses both particles and the available growth volume. There are two minor differences: First, for any next-event time τ the cap-bound particle is displaced deterministically with the growing cap by $\Delta x = v_g \tau$, while the position of the other particle is sampled from the 1D Green's function before Δx is added, as described above. Second, since here both particles can undergo monomolecular reactions with tentative next-event times τ_{s1} and τ_{s2}, the next-event time τ_ν of the domain is the minimum of τ_g, τ_{dd}, τ_{s1} and τ_{s2}.

2.C.3 Summarized cylinder growth sampling algorithm

The concept presented in the preceding sections can be compiled into the following algorithm for growth domain construction in eGFRD.

Starting from the situation in which a growing cylinder with growth velocity v_g and catastrophy rate k_c just exited from its last update we first sample a next-catastrophy time τ_c from an exponential distribution with decay rate k_c. Depending on whether there are particles on and/or close to the cylinder cap, we construct a domain that surrounds the cap and the particles associated or interacting with the cap and the available growth volume in the direction of the growing cylindrical surface. Possible growth domain types are:

- *Cylindrical Surface Cap Growth*: contains only the growing cap, no particles.
- *Cylindrical Surface Growing Cap Single*: contains the growing cap and a cap-bound particle.
- *Cylindrical Surface Growing Cap Interaction*: contains the growing cap and a nearby particle diffusing and drifting on the cylinder.
- *Mixed Pair 1D/Growing Cap*: contains the growing cap, a cap-bound particle and a nearby particle diffusing and drifting on the cylinder.

We then calculate a next-event time τ_g for the growth event which is directly determined by the length of the "free path" L_g available to the growth domain in growth

direction, $\tau_g = L_g/v_g$. If the domain contains a mobile particle that is not bound to the cap, we calculate a next-event time for particle association to the cap (or cap-bound particle) or for exit through the absorbing boundary from the 1D Green's function with drift (section 2.3) in which the drift v is substituted via $v \to (v - v_g)$. In the following this function is denoted by p_{v-v_g}. For all of the above domain types that contain a particle, we finally also compute the next-event time of a monomolecular particle reaction τ_s, where τ_s is the smaller of the two tentative monomolecular reaction times if there are two particles involved. The next-event time for the growth domain then is defined as $\tau_\nu = \min(\tau_c, \tau_g, \tau_{dd}, \tau_s)$; this automatically determines the scheduled next-event type. The possible events produced by growth domains require slightly different update procedures:

- *Cylindrical Surface Catastrophy* ($\tau_\nu = \tau_c$): If the next event is a catastrophy we burst all associated domains and shorten the cylinder down to zero length. The cylindrical single and pair domains that enclose cylinder-bound particles are bursted in the regular fashion; bursting of growth domains, which also contain the growing cylinder end, is described further below.

- *Cylindrical Surface Growth* ($\tau_\nu = \tau_g$): In this case we first extend the length of the growing cylinder by $\Delta L_g = v_g \tau_g$. If the domain contains a cylinder-bound mobile particle, a new particle position x_ν is sampled from $p_{v-v_g}(x, \tau_g)$ and ΔL_g added to x_ν afterwards.

- Particle exit ($\tau_\nu = \tau_{dd}$): here first the length of the cylindrical surface is enlarged by $\Delta L_{dd} = v_g \tau_{dd}$. The cap and an eventual cap-bound particle are displaced by ΔL_{dd}. Then, if the exit of the diffusing cylinder-bound particle is through the reactive boundary, it is removed and a new cap-bound product particle is placed at the updated position of the cap, which will subsequently result in the creation of a *Cylindrical Surface Growing Cap Single*. If the exit is through the absorbing boundary, the sampled new particle position x_ν has to be transformed via $x_\nu \to x_\nu + v_g \tau_{dd}$.

- Particle monomolecular reaction ($\tau_\nu = \tau_s$): again, first the cylinder length should be enlarged by $\Delta L_s = v_g \tau_s$. The cap and an eventual cap-bound particle are displaced accordingly. The new position x_ν of a diffusing particle is sampled from $p_{v-v_g}(x, \tau_s)$ and post-transformed via $x_\nu \to x_\nu + \Delta L_s$. The particle that underwent the monomolecular reaction is placed at contact with the cylinder at a random angle.

- Bursting $\tau \leq \tau_\nu$: If any of the domains is bursted at an arbitrary time τ, the cap and cap-bound particles have to be displaced by $\Delta L = v_g \tau$. For the diffusing particles new positions are sampled from $p_{v-v_g}(x, \tau)$ and ΔL is added afterwards.

Note that growth, binding and monomolecular reaction events are conditioned on the fact that a catastrophy did not yet happen. The above prescription exploits the fact that catastrophy times are Poissonian, which precisely means that the probability of an catastrophy event to happen within the time interval $[t, t + dt]$ is independent of the fact that it did not occur until time t.